Helsinki University of Technology Radio Laboratory Publications
Teknillisen korkeakoulun Radiolaboratorion julkaisuja
Espoo, April 2007 REPORT S 287

ANTENNA PATTERN CORRECTION TECHNIQUES AT SUBMILLIMETER WAVELENGTHS

Ville Viikari

Dissertation for the degree of Doctor of Science in Technology to be presented with due permission for public examination and debate in Auditorium S4 at Helsinki University of Technology (Espoo, Finland) on the 27th April 2007 at 12 o'clock noon.

Helsinki University of Technology
Department of Electrical and Communications Engineering
Radio Laboratory

Teknillinen korkeakoulu
Sähkö- ja tietoliikennetekniikan osasto
Radiolaboratorio

Distribution:
Helsinki University of Technology
Radio Laboratory
P.O. Box 3000
FI-02015 TKK
Tel. +358-9-451 2252
Fax. +358-9-451 2152

ISBN 978-951-22-8713-0 (printed)
ISBN 978-951-22-8714-7 (electronic)
http://lib.tkk.fi/Diss/2007/isbn9789512287147

ISSN 1456-3835

Otamedia Oy
Espoo 2007

ABSTRACT OF DOCTORAL DISSERTATION	HELSINKI UNIVERSITY OF TECHNOLOGY P.O. BOX 1000, FI-02015 TKK http://www.tkk.fi

Author Ville Viikari

Name of the dissertation
Antenna Pattern Correction Techniques at Submillimeter Wavelengths

Manuscript submitted 12.12.2006	Manuscript revised 2.3.2007

Date of the defence 27.4.2007

☐ Monograph	☒ Article dissertation (summary + original articles)

Department Electrical and Communications Engineering
Laboratory Radio Laboratory
Field of research Radio Engineering
Opponent(s) Professor Wolfgang Menzel
Supervisor Professor Antti Räisänen
Instructor

Abstract
Hologram- and reflector-based compact antenna test ranges (CATRs) have shown potential for measurement of large submillimeter wave antennas. However, the measurement accuracy of these ranges needs to be still improved for measuring low side lobe antennas. The measurement accuracy of these ranges can be improved by using antenna pattern correction techniques. Several such techniques have been developed for microwave frequencies but most of them are not directly applicable at submillimeter wavelengths. In this thesis, four antenna pattern correction techniques that are applicable at submillimeter wavelengths are developed: feed scanning based antenna pattern comparison (APC) method, frequency shift method, and two methods that are based on a virtual antenna array. Applicabilities of these methods are studied analytically, and they are verified with simulations and measurements in a hologram-based compact antenna test range at 310 GHz.
The feed scanning based APC is applicable for compact antenna test ranges. In this method, the corrected antenna pattern is obtained from the antenna patterns measured with different range feed locations. The antenna pattern of the antenna under test (AUT) is measured at several frequencies in the frequency shift method. This method, which was originally developed for lower frequencies, is now found to be especially applicable for hologram-based CATRs. The method is able to compensate partially a possible non-ideal operation of the hologram, because a hologram is a dispersive element. Virtual array correction techniques are suitable for far-field and compact ranges. In these methods, the antenna pattern of the AUT is measured at several accurately known locations. These measurements form a virtual antenna array at each rotation angle of the AUT. The array factor of each array is modulated such that it has a constant gain towards the desired signal and high attenuation to other directions. Estimates of the antenna pattern of the antenna under test and the angular interference spectrum of the test range are taken into account in the array synthesis. One method uses an alternating projections method for array synthesis, whereas the other method maximizes the signal-to-interference ratio in the measurement. The correction accuracies of the feed scanning APC and frequency shift method are found to be approximately equal to that of the conventional APC. The correction accuracies of the virtual array methods are found to be much better than that of the APC.

Keywords Antenna measurements, compact range, error compensation, submillimeter wave measurements.

ISBN (printed) 978-951-22-8713-0	ISSN (printed) 1456-3835
ISBN (pdf) 978-951-22-8714-7	ISSN (pdf) 1456-3835
Language English	Number of pages 59 + 54

Publisher Helsinki University of Technology, Radio Laboratory

Print distribution Helsinki University of Technology, Radio Laboratory

☒ The dissertation can be read at http://lib.tkk.fi/Diss/2007/isbn9789512287147

VÄITÖSKIRJAN TIIVISTELMÄ	TEKNILLINEN KORKEAKOULU PL 1000, 02015 TKK http://www.tkk.fi

Tekijä Ville Viikari

Väitöskirjan nimi
Antennin suuntakuvion korjausmenetelmiä alimillimetriaaltoalueella

Käsikirjoituksen päivämäärä 12.12.2006	Korjatun käsikirjoituksen päivämäärä 2.3.2007

Väitöstilaisuuden ajankohta 27.4.2007

☐ Monografia	☒ Yhdistelmäväitöskirja (yhteenveto + erillisartikkelit)

Osasto Sähkö- ja tietoliikennetekniikan osasto
Laboratorio Radiolaboratorio
Tutkimusala Radiotekniikka
Vastaväittäjä(t) Professori Wofgang Menzel
Työn valvoja Professori Antti Räisänen
Työn ohjaaja

Tiivistelmä
Heijastimeen ja hologrammiin perustuvat kompaktit antennimittauspaikat ovat lupaavia keinoja suurten alimillimetri-aaltoalueen antennien mittaamiseen. Näiden mittauspaikkojen mittaustarkkuus on kuitenkin vielä riittämätön hyvin suuntaavien antennien mittaamiseen. Mittauspaikkojen mittaustarkkuutta voidaan parantaa antennin suuntakuvion korjausmenetelmien avulla. Lukuisia korjausmenetelmiä on kehitetty mikroaaltotaajuuksille, mutta useimmat niistä eivät sovellu alimillimatriaaltoalueelle. Tässä työssä on kehitetty neljä erityisesti alimillimetriaaltoalueelle sopivaa antennin suuntakuvion korjausmenetelmää: syötön siirtoon perustuva suuntakuvioiden vertailumenetelmä, taajuuden poikkeutukseen perustuva menetelmä, sekä kaksi menetelmää, jotka perustuvat virtuaaliseen antenniryhmään. Menetelmien käyttökelpoisuutta on tarkasteltu teoreettisesti ja menetelmien toimivuus on varmennettu simuloinnein ja mittauksin hologrammiin perustuvassa antennimittauspaikassa taajuudella 310 GHz.
Syötön siirtoon perustuvassa menetelmässä tutkittavan antennin suuntakuvio mitataan useasti siten, että antennimittauspaikan syöttö on eri paikassa jokaisen mittauksen aikana. Korjattu suuntakuvio lasketaan mitatuista suuntakuvioista. Tässä työssä on osoitettu, että aiemmin mikroaaltotaajuuksille kehitetty taajuuden poikkeutusmenetelmä soveltuu erityisen hyvin hologrammiin perustuvaan kompaktiin antennimittauspaikkaan. Menetelmän avulla voidaan korjata osa hologrammin mahdollisesta epäideaalisesta toiminnasta syntyvistä virheistä. Menetelmässä korjattu suuntakuvio lasketaan usealla eri taajuudella mitatuista suuntakuvioista. Virtuaaliseen antenniryhmään perustuvat menetelmät sopivat kompakteihin- ja kaukokenttämittauspaikkoihin. Näissä menetelmissä tutkittavan antennin suuntakuvio mitataan useassa tarkasti tunnetussa kohdassa antennimittauspaikkaa. Mittaustuloksista muodostetaan virtuaalinen antenniryhmä jokaisella antennin kiertokulmalla. Antenniryhmille syntetisoidaan ryhmäkuviot, joilla on vakiosuuntaavuus halutun signaalin suuntaan ja mahdollisimman pieni suuntaavuus muihin suuntiin. Suuntakuvion synteesissä otetaan huomioon arviot tutkittavan antennin suuntakuviosta ja häiriösignaalien kulmaspektristä. Toisessa korjausmenetelmässä synteesi perustuu iteratiiviseen vuorottelevien projektioiden menetelmään, kun taas toisessa menetelmässä käytetty synteesi maksimoi signaali-häiriösuhteen. Syötön siirtoon perustuvan suuntakuvioiden vertailumenetelmän ja taajuuden poikkeutukseen perustuvan menetelmän mittaustarkkuuden on havaittu olevan samaa luokkaa perinteisen suuntakuvioiden vertailumenetelmän tarkkuuden kanssa. Virtuaalisiin antenniryhmiin perustuvien menetelmien mittaustarkkuuden on havaittu olevan edellisiä parempi.

Asiasanat Alimillimetriaaltoalue, antennimittaukset, kompakti mittauspaikka, virheen korjaaminen

ISBN (painettu) 978-951-22-8713-0	ISSN (painettu) 1456-3835
ISBN (pdf) 978-951-22-8714-7	ISSN (pdf) 1456-3835
Kieli Englanti	Sivumäärä 59 + 54

Julkaisija Teknillinen korkeakoulu, Radiolaboratorio

Painetun väitöskirjan jakelu Teknillinen korkeakoulu, Radiolaboratorio

☒ Luettavissa verkossa osoitteessa http://lib.tkk.fi/Diss/2007/isbn9789512287147

Preface

I have had a great opportunity to work in the same hologram research project since I joined in the Radio Laboratory 2001. This thesis work started in 2003 when I first discovered antenna pattern correction techniques in my master's thesis. I thank my supervisor Professor Antti Räisänen for this opportunity.

Juha Mallat deserves honors for several reasons. Juha has given good comments and ideas about this research. He has designed and manufactured the dielectric-loaded lens antenna with Juha Ala-Laurinaho. Also, he has helped with measurements. Juha Ala-Laurinaho and Janne Häkli I thank for good comments and ideas. Anne Lönnqvist and Tomi Koskinen I thank for their contribution in developing the hologram-based CATR. Veli-Matti Kolmonen and Jari Salo deserve acknowledgements for helping with array synthesis algorithms. The whole personnel of the Radio Laboratory and especially the hologram research group I thank for the good atmosphere. Eino Kahra deserves acknowledgements for designing the reflector-based test antenna and other fine mechanical parts.

I would like to thank the pre-examiners, Professor Edward B. Joy and Dr. Inder J. Gupta, for their valuable comments and suggestions for improving this thesis.

I wish to thank the Foundation of the Finnish Society of Electronic Engineers, Jenny and Antti Wihuri Foundation, KAUTE-Foundation, the Finnish Foundation for Promotion of Technology, and Nokia Foundation for supporting this research.

Finally I thank my wife Meri, who has always supported and encouraged me.

Espoo, March 2, 2007

Ville Viikari

Table of Contents

List of Publications

This thesis is based on the work presented in the following publications:

[P1] J. Häkli, T. Koskinen, A. Lönnqvist, J. Säily, J. Mallat, J. Ala-Laurinaho, V. Viikari, A. V. Räisänen, and J. Tuovinen, "Testing of a 1.5 m reflector antenna at 322 GHz in a CATR based on a hologram," *IEEE Transactions on Antennas and Propagation*, vol. 53, no. 10, pp. 3142 – 3150, Oct. 2005.

[P2] V. Viikari, J. Mallat, J. Ala-Laurinaho, J. Häkli, A. Karttunen, T. Koskinen, A. Lönnqvist, E. Noponen, M. Vaaja, and Antti V. Räisänen, " New pattern correction techniques for submm-wave CATRs," *Proceedings of the European Conference on Antennas and Propagation*, Nice, France, Nov. 6 – 10, 2006, CD-rom, ESA SP-626, paper no. 368102.

[P3] V. Viikari, J. Mallat, J. Ala-Laurinaho, J. Häkli, and A. Räisänen, "A frequency shift technique for pattern correction in hologram-based CATRs," *IEEE Transactions on Antennas and Propagation*, vol. 54, no. 10, pp 2963 – 2968, Oct. 2006.

[P4] V. Viikari, J. Häkli, J. Ala-Laurinaho, J. Mallat, and A. V. Räisänen, "A feed scanning based APC technique for compact antenna test ranges," *IEEE Transactions on Antennas and Propagation*, vol. 53, no. 10, pp. 3160 – 3165, Oct. 2005.

[P5] V. Viikari, V.-M. Kolmonen, J. Salo, and A. V. Räisänen, "Antenna pattern correction technique based on an adaptive array algorithm," accepted with minor revision for publication in *IEEE Transactions on Antennas and Propagation*, 2006.

[P6] V. Viikari and A. V. Räisänen, "Antenna pattern correction technique based on signal to interference ratio optimization," accepted for publication in *IEEE Antennas and Wireless Propagation Letters*, 2006.

Publications [P2]-[P6] are mainly this author's own work. Co-authors have supervised the work and in [P5] Veli-Matti Kolmonen has assisted with the implementation of the adaptive array algorithm.

Publication [P1] is a result of collaborative work. The author has calculated the effect of the non-ideal quiet-zone field on the measured antenna pattern and studied the range reflections by calculating the plane-wave spectrum. In addition, the author contributed to the preparation and execution of the antenna measurements.

In addition to publications [P1–P6], this author has authored and co-authored several publications [1–7] related to the topic of this thesis and presented also several conference talks on this topic [8–11].

List of Symbols

A	True antenna pattern of the reference antenna, real part of the center of the circle
a_i	Amplitude of the *i*th signal
$\mathbf{a}$	Steering vector
B	Imaginary part of the center of the circle
$\mathbf{B}$	Normalization matrix
c	The speed of light [m/s]
D	Diameter of the antenna [m], measured antenna pattern
$\mathbf{D}$	Matrix in the NAPC method
d	Antenna displacement [m], range feed displacement [m], interelement distance [m]
d_i	Path length of the *i*th signal [m]
d_{int}	Feed displacement interval
d_{range}	Feed displacement range
E_{AUT}	Aperture field of the antenna [V/m]
E_d	Electric field strength of the direct signal [V/m]
E_{inc}	Incident electric field [V/m]
E_{NF}	Near-field of the antenna [V/m]
E_{QZ}	Quiet-zone field [V/m]
E_r	Electric field strength of the reflected signal [V/m]
E_{trans}	Transmitted electric field [V/m]
$\mathbf{E}$	Matrix in the NAPC method
$\mathbf{E}_N$	Noise subspace
F	Measured antenna pattern of the reference antenna, antenna pattern measured in place, focal length of the collimating element [m]
F_c	Corrected antenna pattern
$\tilde{F}$	Antenna pattern measured at the distance of d
f_0	Center frequency [Hz]
$\mathbf{G}$	Array response matrix
g	Complex phase factor, element pattern
g_p	Real weighting constants
H	Spectral estimator
H_l	Spatial correlation coefficients
$\mathbf{H}$	Matrix in the adaptive array strategy
$\mathbf{I}$	Identity matrix
K	Number of plane waves
k	Wave number [1/m], integer
k_x, k_y, k_z	*x*-, *y*-, and *z*-components of the wave vector [1/m]
k_{x0}	*x*-component of the wave vector at the center frequency [1/m]
$\vec{k}$	Wave vector [1/m]
L	Number of the elements of the subarray

M	Number of the signals, number of array elements
M_l	Lower limit for the synthesized array pattern
M_u	Upper limit for the synthesized array pattern
N	Number of the sample points
P	Antenna pattern
P_{AF}	Array factor
P_{AP}	Array pattern
P_{AUT}	Antenna pattern of the AUT
P_{COR}	Corrected antenna pattern
P_{meas}	Measured antenna pattern of the virtual antenna
$P_{meas,i}$	Measured antenna pattern at the *i*th position
p	Angular interference spectrum
p_{ef}	Effective angular interference spectrum
$\mathcal{P}$	Projector operator
R	Far-field distance [m], antenna pattern of the probe antenna, radius
R_i	Radius of the *i*th fitted circle
r	Distance [m]
$\mathbf{r}$	Location vector
S	Plane wave spectrum, frequency response
T	Transmittance function of the hologram
$\mathbf{T}$	Matrix in the adaptive array strategy
$\mathbf{U}$	Matrix containing the left singular vectors
$\mathbf{u}_i$	Left *i*th singular vector
$\mathbf{u}_r$	Unit direction vector
$\mathbf{V}$	Matrix containing the right singular vectors
$\mathbf{v}_i$	Eigenvector related to *i*th eigenvalue, right *i*th singular vector
w_n	Weight of the *n*th element
$\mathbf{w}$	Weighting vector
$\mathbf{w}_0$	Initial guess for the element weights
$\mathbf{X}$	Matrix containing the responses of different elements
x, y, z	Position coordinates [m], antenna coordinates [m]
x', z'	Quiet-zone coordinates [m]
x_i	Real part of $P_{meas,i}(\theta_n)$, received signal at the *i*th element
$\mathbf{Y}_1, \mathbf{Y}_2$	Matrices in the matrix pencil method
y_i	Imaginary part of $P_{meas,i}(\theta_n)$
$\mathbf{y}$	Vector in the adaptive array strategy
z_0	Near-field distance of the antenna [m]
z_i	Complex factor related to *i*th signal
α	Horizontal angle of the antenna pattern at the wavelength of λ [rad], Angle of the AUT [rad]
α_0	Horizontal angle of the antenna pattern at the center frequency [rad]
α_i	Damping factor of the *i*th signal [1/Hz]

α_{max}	Maximum horizontal angle, where the correction is performed [rad]
Δf	Deviation from the center frequency [Hz], frequency interval [Hz]
Δl	Path length difference [m]
$\Delta\theta$	The steered direction of the plane wave [rad]
$\Delta\lambda$	Deviation from the wavelength at the center frequency [m]
$\Delta\phi$	Phase variation from the linear phase slope in the quiet-zone [rad]
$\Delta\psi$	Phase change [rad]
ε_r	Relative permittivity
θ	Horizontal angle [rad]
θ_k	Direction-of-arrival of *k*th plane wave
θ_{max}	Maximum angle, in which the correction can be performed [rad]
θ_{min}	Minimum angle, in which the correction can be performed [rad]
θ_n	*n*th angle in the antenna pattern [rad]
θ_{x0}	Offset angle of the hologram [rad]
λ	Wavelength [m]
λ_0	Wavelength at the center frequency [m]
ν	Spatial frequency [1/m]
ν'	Spatial frequency when the feed is displaced [1/m]
Σ	Diagonal matrix containing the singular values
φ	Angle between plane waves [rad]
Ψ_{AUT}	Angular range of the AUT, in which the correction is performed
Ψ_{feed}	Angular range projected to the range feed
ψ_{inc}	Phase of the incident field [rad]
ψ_k	Phase of the *k*th plane wave
ψ_{trans}	Phase of the transmitted field [rad]
$\psi_{trans,N}$	Normalized phase of the transmitted field [rad]
ψ'_{trans}	Phase of the transmitted field when the feed is displaced [rad]

List of Acronyms

APC	Antenna Pattern Comparison
AUT	Antenna Under Test
CATR	Compact Antenna Test Range
CCR	Compensated Compact Range
DOA	Direction-Of-Arrival
ESA	European Space Agency
FFT	Fast Fourier Transform
MST	Modulated Scattering Technique
MUSIC	Multiple Signal Classification
NAPC	Novel Antenna Pattern Comparison
RAM	Radar Absorbing Material
RCS	Radar Cross Section
RF	Radio Frequency

1 Introduction

1.1 Background

The interaction between a matter and submillimeter wave photon occur mainly through changes in thermal, rotational, or bending state of a molecule. Therefore submillimeter waves can be used to detect different molecular species, their concentration, and their physical properties such as heat or pressure. Currently submillimeter wave instruments are used mainly for Earth atmospheric observations and for radio astronomy [12]. In the future submillimeter wave instruments may be used also in biomedical applications, material quality control applications, security control applications, and in demining applications [12].

Several future scientific space missions have on board electrically very large submillimeter wave antennas. For example, the European Space Agency (ESA) is going to launch Planck and Herschel space telescopes in the near future [13]. The Planck has a 1.5-m telescope operating from 27 GHz to 857 GHz. The Herschel has a 3.5-m telescope and its highest operation frequency is 5 THz.

The manufacturing of large submillimeter telescopes is very challenging because of the tight reflector surface accuracy requirement (about one hundredth of a wavelength). The manufacturing inaccuracies may distort the telescope operation and spoil even the whole space mission. Therefore the electrical operation of these telescopes should be verified prior to launch. Measurement techniques of large submillimeter wave antennas are not yet well established, however, but hologram- and reflector-based compact antenna test ranges (CATRs) are among the most potential methods.

The measurement accuracy of a compact antenna test range is limited by the level of the spurious signals. The level of the spurious signal should be much lower than the measured side lobe level of the antenna under test (AUT). Spurious signals are caused by the unwanted reflections in the range. In reflector-based CATRs, also inaccuracies and deformations of the range reflector may cause distortions, because the tight surface accuracy requirements of about a hundredth of a wavelength can not be fully satisfied. The surface accuracy requirement is lower with the hologram. However, the main challenge with large holograms is the current manufacturing technology. Large (> 1m) holograms have to be manufactured from several pieces. The seams and the misalignment between the hologram pieces cause spurious signals and decrease the measurement accuracy.

To mitigate the effects of the spurious signals, several antenna pattern correction and range evaluation techniques have been developed. Most of the techniques have been developed for microwave frequencies and they are not directly applicable at submillimeter wavelengths.

1.2 Scope and Contents of the Thesis

In this thesis, four antenna pattern correction techniques, feed scanning based antenna pattern comparison (APC), frequency shift method, adaptive array-based method, and a method based on signal-to-interference ratio optimization have been developed. The methods are especially suitable at submillimeter wavelengths. The feed scanning based APC can be used in a reflector-based CATR as well as in a hologram-based CATR. The frequency shift method suits best for hologram-based CATRs whereas the adaptive array based technique and the

technique based on signal-to-interference ratio optimization are suitable for far-field and compact antenna test ranges.

This thesis is organized as follows: possible submillimeter wave antenna measurement techniques are reviewed in Chapter 2. Chapter 3 gives a survey of previously developed antenna pattern correction techniques and introduces stray signal imaging techniques, which are used to improve antenna test ranges. The antenna pattern correction techniques that have been developed in this thesis are briefly introduced in Chapter 4. The conclusions are presented in Chapter 5.

1.3 New Scientific Results

The thesis contains the following new scientific results:

1) The performance of the antenna pattern correction technique based on adaptive array algorithm has been improved by implementing a method for maximizing the signal-to-interference ratio.

2) New antenna pattern correction technique based on adaptive array algorithm has been developed.

3) The frequency shift method has found to be especially applicable in hologram-based compact antenna test ranges.

4) New antenna pattern correction technique based on range feed scanning has been developed.

5) The effect of the non-ideal quiet-zone field on the measured antenna pattern has been estimated at 310 GHz.

2 Antenna Pattern Measurement Techniques at Submillimeter Wavelengths

Submillimeter wave antennas are not yet being tested extensively and therefore suitable measurement techniques are not well established. There are several proposed techniques, but only some of them have been used in practice. The proposed techniques are reviewed, e.g., in [14].

2.1 Antenna Characteristics

An antenna transforms guided electromagnetic waves into free space radiation and vice versa. The field produced by an antenna is generally divided into near-field and far-field regions [15]. The near-field region is still subdivided into a reactive near-field and a radiating near-field. The field components which decay exponentially are strongly present in the reactive near-field, which is often defined to reach to a distance of $\lambda/2\pi$ from the antenna but may in some antenna structures extend to a distance of several wavelengths (λ). The radiating near-field is beyond the reactive near-field and it mainly consists of the field components, which decay proportional to $1/r$. The far-field of the antenna is reached at a distance (an often used definition)

$$R = \frac{2D^2}{\lambda}, \tag{2.1}$$

where D is the diameter of the antenna and λ is the wavelength. In the far-field, the field is proportional to $\frac{e^{-jkr}}{r}$, i.e., the directional properties of the antenna do not depend on the distance in the far-field region. As antennas are generally designed to operate in the far-field region, the antenna characteristics are measured in the far-field conditions.

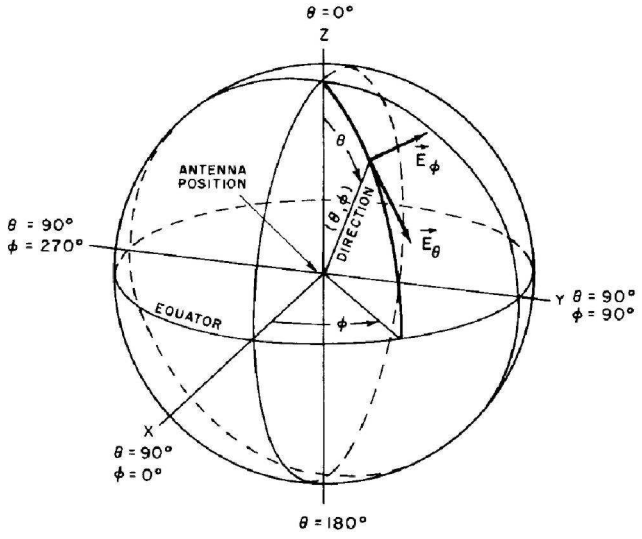

Fig. 2.1. The standard coordinate system in antenna measurements [15].

Usually antennas are characterized in terms of their directional properties. The antenna pattern describes the radiated field (amplitude, phase, and polarization) by an antenna as a function of

the antenna pointing angle. The antenna pattern is typically represented in a standard spherical coordinate system [15], see Figure 2.1. When measuring high-gain antennas, it is desirable to orient the main beam axis to the equator.

2.2 Far-Field Technique

In the far-field range the distance between the probe antenna and the antenna under test is so large that the spherical wave front radiated by the probe antenna is practically a plane wave in the aperture of the antenna under test. The required distance between the probe and the AUT depends on the size of the AUT, the wavelength, and the desired measurement accuracy. Generally the distance defined in (2.1) is required. At this distance, a spherical wave front has a maximum deviation of $22.5°$ from a plane wave in the aperture of the AUT, when the AUT is pointed to the source. When measuring low-side lobe antennas, even larger distance is needed, such as $4D^2/\lambda$ or $8D^2/\lambda$ [16].

The required distance becomes impractically large at submillimeter wavelengths for large antennas. For example, the required distance must be at least $R = 6.7$ km for an antenna with $D = 1$ m at 1 THz. However, the atmospheric attenuation may be from tens to hundreds of decibels per kilometer. In addition, temperature gradients and humidity variations may cause fluctuations to the attenuation in the signal path. Due to the above reasons, the far-field range is suitable for measuring only very small antennas at submillimeter wavelengths.

2.3 Near-Field Technique

In the near-field measurements, the electrical field is first probed close to the antenna under test. The far-field characteristics of the AUT are then computed from the measured near-field data [17]. The electrical field is probed on a plane, on a cylinder, or on a sphere. The field can also be probed on an elliptic cylinder, on a parabolic cylinder, or on a sphere in conical surface coordinates, but these geometries are mechanically more difficult to achieve. The antenna pattern can be calculated only in the directions, where the probed surface entirely covers the AUT. Therefore the spherical near-field scanning is the only generally used geometry that provides full information about the antenna pattern, although it would be possible to use other geometries such as, e.g., cubic near-field scanning. However, the planar scanning is preferred when measuring directive antennas. Commonly planar scanning is done in rectangular coordinates, but plane-polar and bi-polar geometries can be used as well [18], [19].

In order to prevent spatial aliasing, the spatial sampling interval has to be dense enough. The fundamental sampling interval for planar-rectangular scanning is $\lambda/2$. If the antenna pattern is calculated only in a certain restricted angular region, a larger sampling interval may be used. In that case the probe antenna has to be chosen properly to filter out the aliasing field components. The effect of the probe antenna is usually taken into account in the near-field to far-field transformation. For planar-rectangular sampling the probe corrected antenna pattern is calculated from

$$P(k_x, k_y) = \frac{e^{-jk_z z_0}}{2\pi} R^{-1}(k_x, k_y) \cdot \int_{-\infty}^{\infty}\int_{-\infty}^{\infty} E_{NF}(x, y, z_0) e^{-j(k_x x + k_y y)} dxdy \,, \tag{2.2}$$

where k_x, k_y and k_z are the *x*-, *y*-, and *z*-components of the wave vector $\vec{k}$, $R(k_x, k_y)$ is the antenna pattern of the probe and $E_{NF}(x, y, z_0)$ is the near-field of the antenna at the distance of z_0 [17]. The transformation can be effectively performed with the fast Fourier transform (FFT) algorithm. The computing time with the FFT is proportional to $N^2 \log_2 N$, where N is the number of sample points.

There are several challenges with near-field measurements at submillimeter wavelengths. The non-planarity of the scanner introduces phase errors to the measured near-field. General criterion for the scanner planarity is $\lambda/100$. The planarity requirement may be mitigated by measuring the position of the probe and correcting the measured phase respectively [20] or by using a servomechanism to adjust the probe position accurately.

Another challenge is the RF cables, which flex during scanning. The electrical length of the cable changes when the cable is flexed, and therefore also the phase of the measured field is changed. Several techniques for measuring the phase error caused by the cable flexing are introduced in [21]. In [22], Säily et al. introduce a system for measuring and correcting the phase errors due to cable flexing. Error and uncertainty analysis for the planar near-field measurements is presented in [23].

Near-field measurement times may be very long because a very large number of the near-field samples is required for characterizing a large submillimeter wave antenna. For example, about 36 million samples are needed for 1.5 x 1.5 m^2 scanning area at 600 GHz (satisfying the fundamental sampling criterion of $\lambda/2$). The complete scanning of such an area would take 21 days at the sampling rate of 20 samples per second. This sets high stability requirements for the measurement instruments.

Despite these challenges, near-field measurements are performed at relatively high frequencies. For example, near-field measurement of a 1.6-m antenna at 650 GHz is reported in [24]. The scanning area is 2.4 by 2.4 m^2 and the measured scanner rms planarity is 4 μm. Another near-field measurement at 550 GHz is reported in [25].

2.3.1 Modulated Scattering Technique

The antenna pattern of the AUT can be potentially measured faster with the modulated scattering technique (MST) [26], than with the conventional near-field probing. The MST employs an array of scattering probes instead of one mechanically moved probe. The near-field of the AUT is obtained by measuring the AUT response to the different scattering probes. The array of scattering probes is illuminated with the AUT in a monostatic case or with an auxiliary antenna in a bistatic case. The MST has been demonstrated at microwave frequencies.

2.3.2 Holographic and Phase Retrieval Techniques

Some challenges related to the near-field phase measurements can be avoided by exploiting holographic or phase retrieval techniques. In these techniques, the phase data is obtained indirectly from the measured amplitude data. In Gabor holography, the field produced by the AUT is interfered with an accurately known reference signal and the field produced by the AUT is obtained by subtracting the reference field from the measured interference amplitude data. Holographic testing of terahertz antennas is numerically studied in [27].

Another possibility to obtain the phase from the amplitude data is to exploit iterative phase retrieval algorithms, such as plane-to-plane diffraction algorithm [28] or conjugate-gradient method [29], [30]. The methods utilize amplitude data measured on two adjacent planes with sufficient separation [29], amplitude data measured with two dissimilar probes [30] or amplitude data with a priori information about the AUT [31]. Experimental tests of the algorithms at microwave frequencies are introduced in [28], [29], [32], and [33]. The feasibilities of the plane-to-plane diffraction algorithm and the conjugate-gradient method have been verified at submillimeter wavelengths and a combined algorithm is proposed for accelerated convergence in [8].

Most of the phase retrieval algorithms require two sets of near-field data. Therefore these techniques do not seem attractive for measuring large submillimeter antennas whose near-field scanning is very time-consuming.

2.4 Defocusing Technique

Usually antennas are focused at infinity, and therefore the antenna pattern measurement must be performed in the far-field defined by (2.1). However, a reflector antenna may be approximately defocused at a specific distance instead of infinity by displacing its feed. Then the antenna pattern measurement can be performed relatively close to the AUT [34] (Figure 2.2).

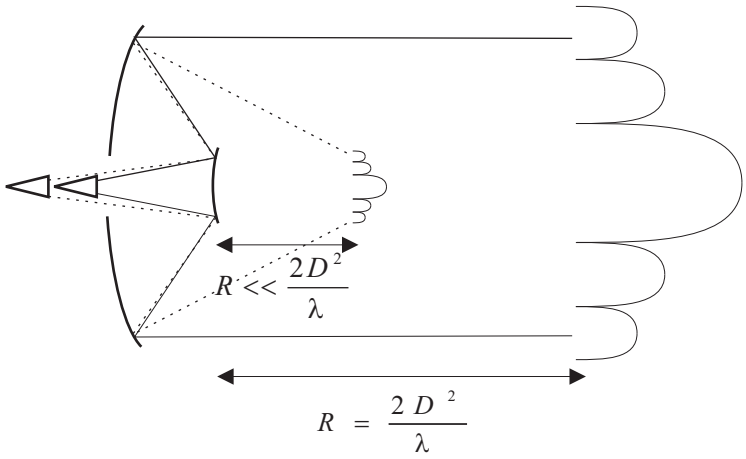

Fig. 2.2. The principle of the defocusing technique [14].

A parabolic mirror can not be focused exactly at a point at finite distance, but an elliptical mirror would be needed for that. Because the parabolic surface deviates from the elliptical one, there exists phase aberration, i.e., the path lengths from one focal point to another are not equal. Due to the phase aberration, the antenna pattern of the defocused reflector slightly differs from the antenna pattern focused at infinity and mathematical manipulation is needed for obtaining the true pattern from the defocused pattern. The defocusing technique is not suitable for all antennas, as there must be a possibility to move the antenna feed. The defocusing technique has been proposed as a potential measurement technique at THz frequencies [14], but no measurements at submillimeter wavelengths or higher frequencies are published.

2.5 Combined Physical and Mechanical Measurements

It is suggested, that terahertz antennas could be characterized by a combination of physical and electrical measurements [14]. The characterization is done with a simulation model, which consists of a physically measured reflector surface shape and an electrically measured antenna feed pattern. The shape of the reflector is measured either mechanically or optically. Mechanical machines may achieve accuracies up to 2 – 5 μm, peak-to-peak, for 2 – 3 m antenna structures [35]. The distance repeatability of optical devices is few micrometers and the angular repeatability is approximately 20 μm for a 2-meter object [36].

Both the amplitude and the phase pattern of the antenna feed have to be measured. In addition, the location of the physical phase center and the alignment of the feed with respect to the reflector have to be accurately known. As the feed is electrically relatively small, it can be measured for example in a far-field range.

There are several challenges with this method. First of all, it is difficult to take multiple reflections into account in the simulation model. Another challenge is to physically measure the position of the phase center and the alignment of the feed accurately enough. Thirdly, a very large number of physical measurement points is needed to precisely model the reflector surface. Usually the number of the measurement points is so small that the antenna radiation can be predicted only in a narrow angular region. In addition, this method can not be regarded as reliable antenna characterization technique as the electrical end-to-end techniques.

Antenna characterizations based on physical measurements are described in [37], and [38]. Both antennas are 1.5 meter in diameter and their operations have been simulated at 100 GHz and 503 GHz, respectively.

2.6 Compact Antenna Test Ranges

In a compact antenna test range (CATR), a plane wave field used for antenna testing is generated with a lens, a reflector, or a hologram. The antenna pattern of the AUT is measured by rotating the antenna under test in the plane wave. The advantage of the compact range is that the plane wave conditions needed for antenna testing can be generated in a short distance. A compact antenna test range can be placed in a controlled environment and most of the challenges that are related to atmospheric issues can be avoided.

2.6.1 Reflector-Based CATR

The reflector-based CATR was introduced in the 1960's by Johnson [39]. Nowadays reflector CATRs are widely used for antenna and radar cross section (RCS) measurements up to 200 GHz. A typical reflector-based CATR is shown in Figure 2.3.

Reflector-based CATRs are generally based on one or two offset reflectors. Dual reflector CATR is typically based on a parabolic main reflector and an elliptic subreflector, but it can also be based on two parabolic cylindrical mirrors or on two shaped reflectors.

The lowest operation frequency of the reflector is limited by the edge diffraction, whereas the highest operation frequency is limited by the surface accuracy of the reflector [40]. The deviations of the reflector surface from the ideal surface cause phase errors to the reflected field. Usually a surface accuracy of $\lambda/100$ is required [40].

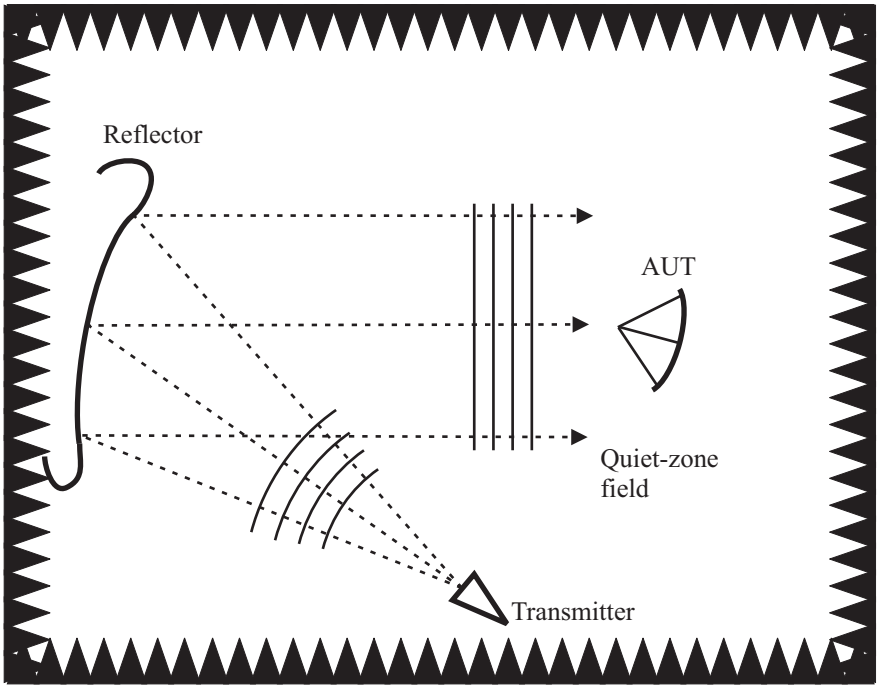

Fig. 2.3. A geometry of a CATR based on a single offset reflector.

The quiet-zone size is limited by the edge diffraction of the reflector. The edge diffraction is generally decreased by applying edge serrations, rolling the edges of the reflector [41], [42] or using a resistive film in the edges of the reflector [43]. Edge diffraction effects may also be decreased by using a dual-reflector feed system for shaping the reflector illumination [44]-[46]. The quiet-zone size is typically 30 % of the main reflector size in single reflector CATRs. Dual reflector CATRs enable a larger quiet-zone, up to 70 % of the main reflector size.

In a single reflector CATR, the cross-polarization level may be too high for measuring low cross-polarization antennas. A dual reflector CATR can be designed so that the reflectors do not cause cross-polarization. This type of cross-polarization free range is called a compensated compact range (CCR).

The main challenge of reflector-based CATRs at submillimeter wavelengths is the required reflector surface accuracy. For example, the surface accuracy requirement is 5 μm at 600 GHz for random distortions. The accuracy should be even better than that if the surface distortion is periodic. Large reflectors need to be assembled from several panels, and the alignment of the panels within the required accuracy is very challenging. Practical measurements of a 1.5-m antenna in a reflector-based CATR at 203, 322, and 503 GHz are described in [38].

2.6.2 Semi-CATRs

In a semi-compact antenna test range, the response of the AUT to a cylindrical wave front is measured [47]. The antenna response to a plane wave is then calculated using a Fourier transform. The cylindrical wave is generated with a parabolic reflector, which is curved in one dimension only.

It is suggested in [48], that the antenna pattern is measured closer to the AUT than is required by the general far-field criterion in (2.1). As the test zone field can be deduced from the range

distance, the measured antenna pattern can be corrected for the finite measurement distance. These techniques have not been used at submillimeter wavelengths.

2.6.3 Lens-Based CATR

In a lens-based CATR, the plane wave needed for antenna testing is generated with a dielectric lens [49], [50]. Geometry of a lens-based CATR is shown in Figure 2.4.

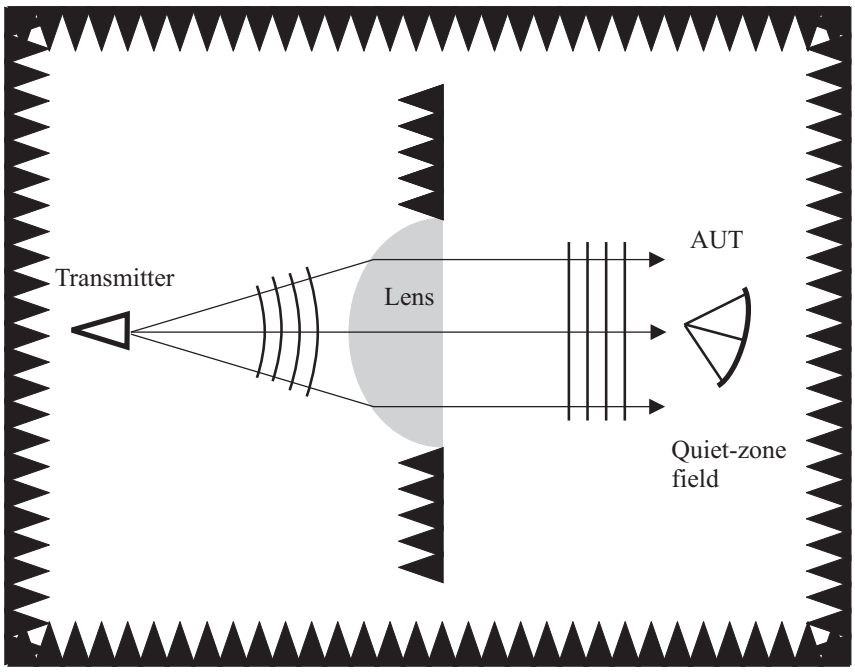

Fig. 2.4. A geometry of a lens-based CATR.

The lens surface is shaped from one side or from both sides. Two shaped surfaces allow modulating both the amplitude and the phase of the transmitted field, whereas one shaped surface can be used to modulate only one of those, usually the phase. The main advantage of a lens over a reflector as a collimating element is the lower surface accuracy requirement (relaxed with a factor of $\sqrt{2}/\left(\sqrt{\varepsilon_r}-1\right)$). Low relative permittivity of the lens enables low surface accuracy requirement. The drawback is that the lower is the relative permittivity the thicker is the lens.

The edge diffraction effects of the lens can be decreased by inserting a serrated metal sheet on the reflector surface [51]. Another theoretical possibility is to modulate the amplitude by controlling the loss of the lens material. The main challenges of lens-based CATRs are related to the lens material. It is difficult to find sufficiently homogeneous and low-loss material that is easy to shape. Lens-based CATRs have not been used at submillimeter wavelengths.

2.6.4 Hologram-Based CATR

In a hologram-based CATR, a hologram is used as a collimating element [52], Figure 2.5. Usually a transmission-type amplitude hologram is used as a collimating element, but it can also be a reflection-type amplitude hologram [1], a transmission-type phase hologram [2] or a reflection-type phase hologram [3]. Amplitude holograms consist of a diffractive grating, which transform incident spherical wave front into a plane wave. Holograms can also be used

for producing other field distributions than plane waves, such as Bessel beams or electromagnetic vortices [2], [4]. The binary hologram grating pattern is generated with a computer and the hologram is manufactured by etching the grating pattern on a copper-plated Mylar-film. The film is stretched on a frame in order to achieve a good planarity.

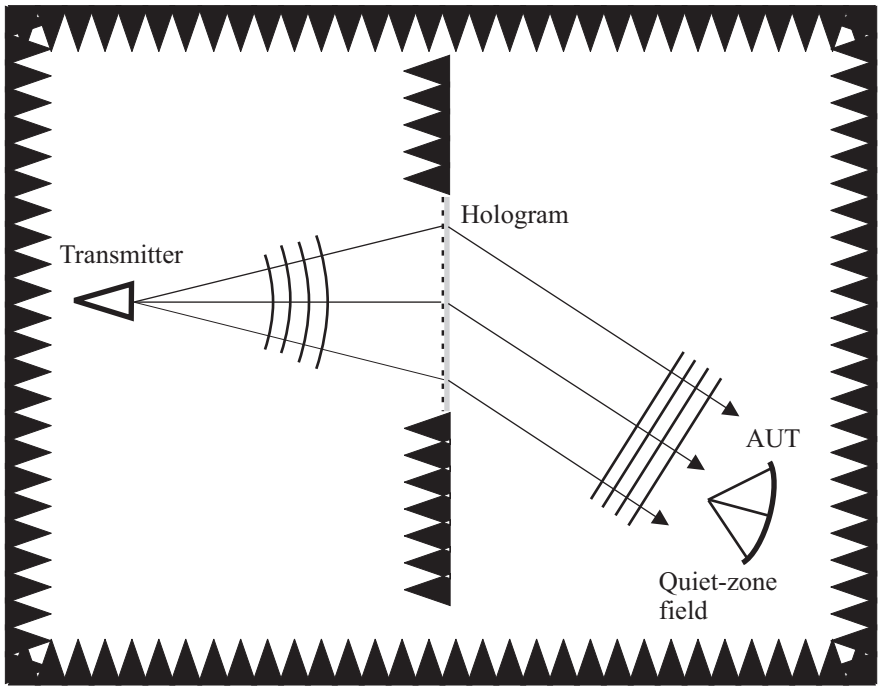

Fig. 2.5. A geometry of a CATR based on a transmission-type hologram.

The advantages of a hologram over a reflector as a collimating element are that a hologram is less expensive and it potentially produces a better quiet-zone. The accuracy requirement of the hologram pattern ($0.01-0.02\lambda$, [53]) is equal to the accuracy requirement of the reflector surface. However, manufacturing of the hologram pattern may be more accurate since conventional printed circuit techniques can be used instead of mechanical milling of the reflector surface. Due to this manufacturing technology, a hologram is inexpensive compared to a reflector. As a planar structure, hologram is also light weight and therefore a hologram-based CATR can be constructed at the site of the antenna under test. In addition, the hologram can modulate both the amplitude and the phase of the transmitted field, and therefore the edge diffraction of a hologram can be controlled better than that of a reflector.

A hologram is a dispersive element, which is designed to operate at a certain frequency. Therefore, holograms have a relatively narrow bandwidth, generally 5-10 % [53]. In order to prevent unwanted diffraction modes from disturbing the quiet-zone field, the plane wave generated by the hologram is usually designed to leave the hologram under an angle of $33°$. Due to this offset angle, the hologram causes cross-polarization, as does an offset reflector as well. In addition, the hologram pattern of an amplitude hologram consists of curved vertical slots on metal. As the transmission of the slot depends on the polarization, the hologram operation can be optimized at one linear polarization only. However, the hologram can be used at both polarizations by employing a dual reflector feed system [54]. The hologram basically modulates the incident field by removing parts of it. Therefore the efficiency of the hologram (received/transmitted power ratio) is relatively low, generally –10 dB.

A hologram-based CATR has been extensively studied for characterizing a large submillimeter wave antenna. A quiet-zone testing of a hologram CATR at 322 GHz is presented in [5] and measurements of a 1.5-m antenna in the same CATR are presented in [P1], [6]. Antenna pattern measurement of Swedish Odin-telescope at 119 GHz in a hologram CATR is reported in [55]. The hologram operation at 650 GHz has been demonstrated in [56].

2.6.5 Radar Cross-Section Measurements

It is suggested in [57] that an antenna pattern of a submillimeter wave antenna could be measured with a radar cross-section measurements in a compact antenna test range [58]. In this technique, a radar cross-section of the AUT is measured with different input impedances of the AUT. The advantages of this technique are that no gain standard or disturbing feed lines are needed. A disadvantage of the method as compared to a one-way measurement is a decreased dynamic range, and therefore this method is suitable for measuring only the main beam of high-gain antennas.

2.7 Antenna Diagnostic

The performance of a submillimeter reflector antenna is usually limited by its reflector surface accuracy. Large reflectors are generally assembled from several rigid panels. In such a case, the antenna operation may be enhanced by improving the alignment of the surface panels. As the deviations from the ideal parabolic surface of the reflector introduce phase variations to the antenna aperture field, the panel alignment can be determined from the antenna aperture field. In the near-field measurements, the surface deviations of the reflector from the ideal parabolic surface are readily seen in the measured phase front. The aperture field of the antenna can be obtained from the far-field pattern as well using inverse Fourier-transform. This is sometimes called a holographic technique, as both the amplitude and phase of the far-field pattern are needed [59]. The aperture field of the antenna can also be calculated from the measured far-field pattern if a priori information about the antenna is available [60]. A holographic diagnostic of a 12-m millimeter-wave antenna is presented in [61].

3 Antenna Pattern Correction and Stray Signal Imaging Techniques

The measurement accuracy of a compact antenna test range is limited by the level of the spurious signals. The level of the spurious signals compared to the level of the desired signal should be much lower than the measured side lobe level of the antenna under test. This condition is difficult to fulfill at submillimeter wavelengths. First of all, submillimeter wave antennas tend to be electrically very large and therefore they may have extremely low side lobes. In addition, a good quality plane wave, which is needed for the antenna testing is challenging to generate. At submillimeter wavelengths the plane wave quality is dominated by the surface accuracy of the collimating element of the CATR. Spurious signals may also be caused by the edge diffraction of the collimating element and the multiple reflections between the range collimating element and the antenna under test.

To overcome these challenges, several antenna pattern correction techniques have been introduced. These techniques are able to partly compensate the effects of the spurious signals and thus also improve the measurement accuracy in an antenna test range. The techniques may be divided into three categories according to what additional information the correction is based on. The techniques in the first category utilize the measured quiet-zone field for pattern correction, the techniques in the second category employ the time- or frequency response of the test range, and the techniques in the third category are based on the spatial response of the test range. A review of antenna pattern correction techniques is presented in [P2]. This Chapter presents techniques from each category and discusses their suitability at submillimeter wavelengths. In addition, stray signal imaging techniques that can be used to map and mitigate stray signals in antenna test ranges are presented in the end of this Chapter.

3.1 Techniques Utilizing the Measured Quiet-Zone Field

3.1.1 Deconvolution Technique

The true antenna pattern of the AUT can be calculated from the measured pattern if the quiet-zone field is known [62], [63]. The quiet-zone field may be measured either by measuring the antenna pattern of an accurately known reference antenna in the quiet-zone field or by probing the quiet-zone field with a small probe antenna. Let us first consider the method with a reference antenna. A reference antenna, whose true antenna pattern is $P(\theta)$, is measured in a test range, whose plane wave spectrum is $S(\theta)$. The measured antenna pattern is

$$D(\theta) = P(\theta) \otimes S(\theta), \tag{3.1}$$

where $\otimes$ indicates a convolution process. Similarly, if the antenna under test, whose true antenna pattern is $A(\theta)$, is measured in the same test range, the measured antenna pattern is

$$F(\theta) = A(\theta) \otimes S(\theta). \tag{3.2}$$

The true antenna pattern of the AUT can be solved from (3.1) and (3.2) by using deconvolution.

Let us next consider the deconvolution method with a probed quiet-zone field. The measured antenna pattern can be calculated from

$$F(\theta) = \int E_{AUT}(x) E_{QZ}(x) \cdot e^{-jk_x(\theta)x} dx \,, \tag{3.3}$$

where $E_{AUT}(x)$ is the aperture field of the antenna under test, $E_{QZ}(x)$ is the quiet-zone field and $k_x(\theta)$ is the x-component of the wave vector as a function of the horizontal angle θ. For simplicity, the previous formula is presented for one-dimensional case, the extension to two-dimensional case being straightforward. The true antenna pattern can be calculated from the aperture field of the AUT, which is first solved from (3.3). The deconvolution technique has been demonstrated at 12 GHz [64].

3.1.2 Other Techniques

Other techniques, which utilize information about the quiet-zone field, are presented in [65], [66]. In these techniques, the quiet-zone field is probed on a sphere enclosing the test object. The effect of a non-ideal quiet-zone field is numerically removed from the measured antenna pattern of the AUT. These techniques have been demonstrated at 9.33 GHz.

3.2 Time and Frequency Techniques

The correction techniques of this category utilize time or frequency response of the antenna test range, i.e., the time or frequency response of the AUT in the test site is measured. Time and frequency responses contain the same information, and therefore time and frequency techniques share the same principle. These techniques separate multipath signals from each other according to time delay (time-domain) or different phase change (frequency domain) due to different signal path lengths. The frequency shift technique, time gating, matrix-pencil method, Gabor transform method, and channel equalization methods fall in to this category.

3.2.1 Frequency Shift Technique

In the frequency shift technique, the antenna pattern is measured several times at different frequencies [67]. As the path lengths of the direct signal and reflected signals differ, the reflected signals are added in different phase to the direct signal at each frequency. The reflectivity level of the test range can be determined from the variations between the measured signals and the corrected antenna pattern is obtained by averaging the measured signals at different frequencies. It is assumed that the characteristics of the antenna under test and the measurement equipment remain unchanged in the whole frequency band.

3.2.2 Time Gating

In the time gating, the range feed transmits a short pulse. If the path lengths of the direct and spurious signals differ, the signals have different delay when arriving at the receiver. The multipath signal components are solved in time domain. The principle of the time gating system is presented in Figure 3.1.

The gating system may be soft or hard. In the soft gating, the measurements are performed in the frequency domain and the time domain data are obtained via inverse Fourier-transform. The hard gating is based on time domain measurements. An implementation of the time gating at microwave frequencies is presented in [68].

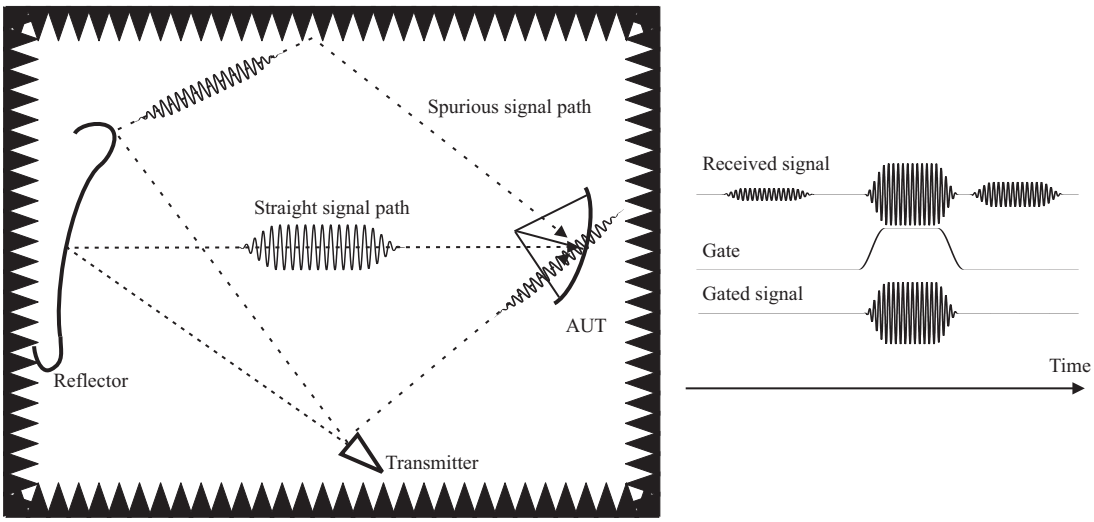

Fig. 3.1. The spurious signals are gated out using a fast switch in the time gating.

In order to separate multipath signals from each others, the pulse length should be smaller than the arrival time differences due to path length differences between the multipath components. The smaller is the pulse length the better is the spatial resolution and thus also the correction accuracy. However, the pulse width is limited by the bandwidth of the equipment and the antenna under test. The shorter is the pulse the larger is its bandwidth. In the hard gating, the pulse repetition rate has to be small enough, so that the reflections between adjacent measurements do not mix. In the soft gating, the pulse repetition rate is determined by the frequency interval, which has to be small enough.

3.2.3 Matrix-Pencil Method

The matrix-pencil method can be used for range evaluation [69] and antenna pattern correction [70]. Instead of the Fourier transform, this technique utilizes the matrix-pencil method [71] for obtaining the time response of the measured frequency response. The advantage with the matrix-pencil method over the Fourier transform is potentially more accurate estimate of spurious signal parameters. The technique is demonstrated below 1 GHz frequency.

The matrix-pencil method is briefly reviewed in the following. Let us consider an antenna pattern measurement in an antenna test range with multipath propagation. The received signal at one antenna rotation angle consists of a direct signal and spurious signals and its frequency response is given as:

$$S(f) = \sum_{i=1}^{M} a_i e^{(\alpha_i + j2\pi d_i / c) f} \quad , \tag{3.4}$$

where a_i are the amplitudes, α_i are the damping factors, and d_i are the path lengths of the multipath signals, M is the number of the signals and c is the speed of light. The measurement is done at N frequency points $f_k = k\Delta f$, $k = 0,1,...,N-1$ and thus (3.4) can be written as:

$$S(k) = \sum_{i=1}^{M} a_i z_i^{k\Delta f} \quad . \tag{3.5}$$

The z_i's are solved from the equation

$$\left\{\mathbf{Y}_1^{+}\mathbf{Y}_2 - z_i\mathbf{I}\right\}\mathbf{v}_i = 0\,, \tag{3.6}$$

where $\mathbf{I}$ is an identity matrix, $\mathbf{v}_i$ is the eigenvector of equation $\mathbf{Y}_2 - z_i\mathbf{Y}_1 = 0$, $^{+}$ denotes the pseudo-inverse, and $\mathbf{Y}_1$ and $\mathbf{Y}_2$ are given as

$$\mathbf{Y}_1 = \begin{bmatrix} S(0) & S(1) & \cdots & S(L-1) \\ S(1) & S(2) & \cdots & S(L) \\ \vdots & \vdots & \ddots & \vdots \\ S(N-L-1) & S(N-L) & \cdots & S(N-2) \end{bmatrix} \tag{3.7}$$

and

$$\mathbf{Y}_2 = \begin{bmatrix} S(1) & S(2) & \cdots & S(L) \\ S(2) & S(3) & \cdots & S(L+1) \\ \vdots & \vdots & \ddots & \vdots \\ S(N-L) & S(N-L+1) & \cdots & S(N-1) \end{bmatrix} \tag{3.8}$$

where L is a free parameter (in presence of noise, $L = N/2$ gives optimal results). After solving z_i's, the amplitude coefficients are solved from

$$\begin{bmatrix} S(0) \\ S(1) \\ \vdots \\ S(N-1) \end{bmatrix} = \begin{bmatrix} 1 & 1 & \cdots & 1 \\ z_1 & z_2 & \cdots & z_M \\ \vdots & \vdots & \ddots & \vdots \\ z_1^{N-1} & z_2^{N-1} & \cdots & z_M^{N-1} \end{bmatrix} \begin{bmatrix} a_1 \\ a_2 \\ \vdots \\ a_M \end{bmatrix}. \tag{3.9}$$

3.2.4 Other Techniques

Fourestie et. al have also presented a method, in which the multipath signal parameters are solved from the measured frequency response using oversampled Gabor transform [72]. The performance of this method is shown to be better than that of the matrix-pencil method. Also this technique has been demonstrated below 1 GHz frequency.

In the technique based on channel equalization, the response of the AUT to a special time domain sequence is measured at each angle [73]. Due to multipath propagation in the test range, the received sequence differs from the transmitted one. A channel model of tapped delay lines is created by comparing the received and the transmitted sequences. Finally the measured pattern is corrected with an adaptive equalizer, which compensates the multipath effects.

3.3 Spatial Techniques

The techniques in this category utilize spatial response of the antenna test range. These techniques separate the spurious signals from the direct signal according to their different spatial frequencies. These techniques include the antenna pattern comparison (APC), feed

scanning based APC, novel antenna pattern comparison (NAPC), virtual array, and adaptive array strategy.

3.3.1 Antenna Pattern Comparison

Originally, the antenna pattern comparison technique is used for determining the reflectivity level of an anechoic chamber [74], but the method can also be used for antenna pattern correction. Let us consider a compact antenna test range, where the quiet-zone field consists of a direct signal and of a reflected spurious signal (Figure 3.2).

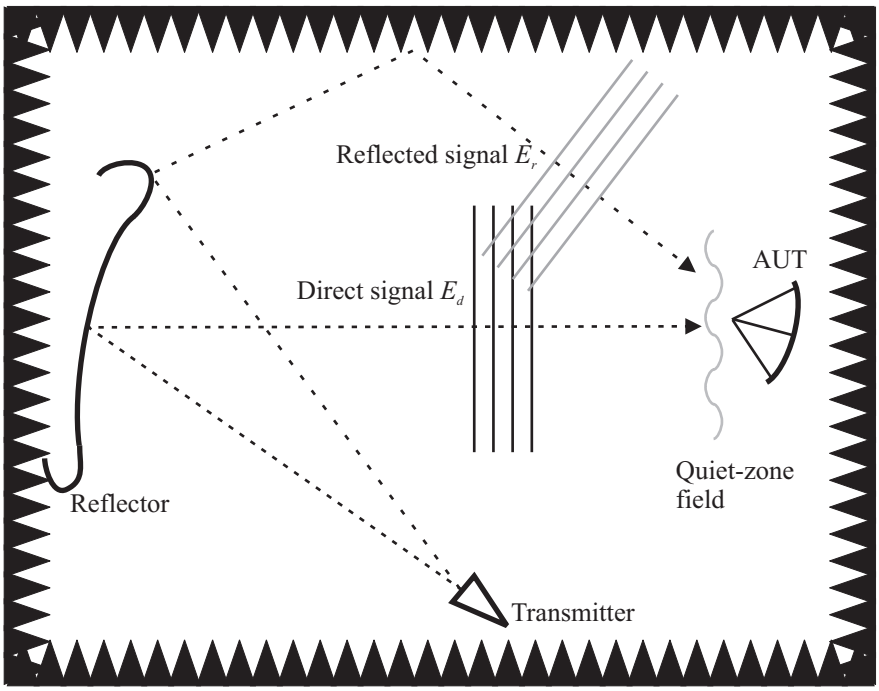

Fig. 3.2. A compact antenna test range with a direct signal and a reflected signal.

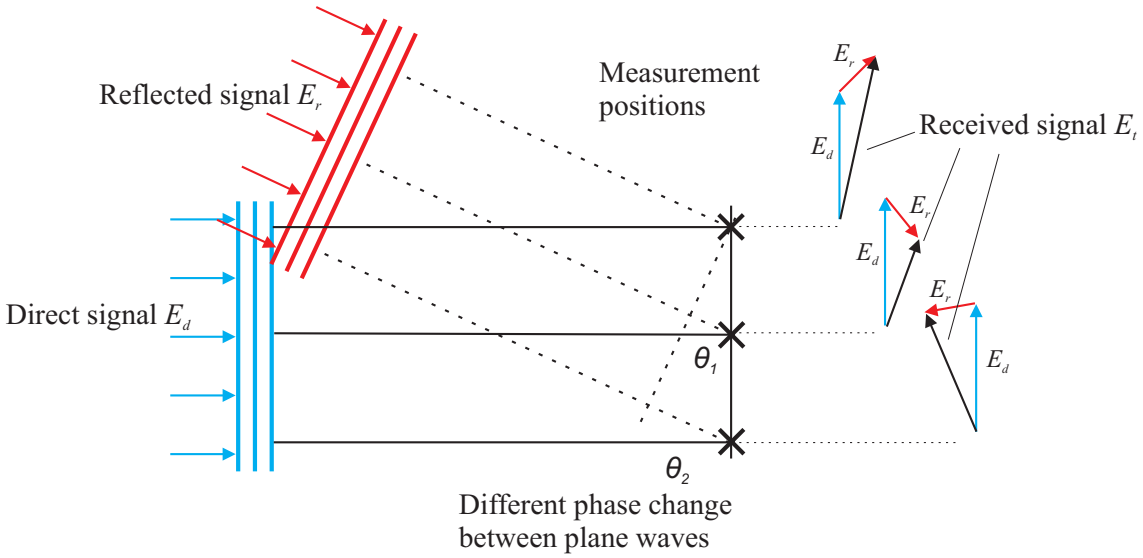

Fig. 3.3. Different phase change of the direct and the reflected signal in the APC technique.

In the APC technique, the antenna pattern of the antenna under test is measured several times at different positions in the quiet-zone. In each point, the received signal is a vector sum of the direct and the reflected signal. As the spatial frequencies of the direct and reflected signals differ, they are added in different phase at each measurement point (Figure 3.3).

The corrected antenna pattern can be obtained for example by averaging the measured signals in each antenna rotation angle. The reflectivity level of the test range can be calculated from the variations between the measured antenna patterns.

3.3.2 Virtual Array

It is assumed in the virtual array method that when measuring the antenna pattern of a directive antenna, the received signal at each measurement angle is a vector sum of the desired signal and one dominating stray signal. The desired signal is received through a side lobe of the antenna under test, whereas the dominating stray signal is received through the high-gain main beam. In the virtual array method, the antenna pattern is measured twice at different positions in the quiet-zone [75]. The antenna is kept in place during the first measurement, whereas it is displaced as a function of the rotation angle during the second measurement. The displacement in the second measurement is adjusted such that the relative phase difference between the desired signal and the stray signal is changed by 180°. The corrected antenna pattern is then obtained by adding the measured signals such that the desired signals add in phase whereas the stray signals add out of phase. Effectively, at each rotation angle, the measurement points form a virtual antenna array, whose array factor has a peak in the direction of the desired signal and a null in the main beam direction. In his paper, Mitchell suggests that for improved performance three or four measurement positions should be used instead of two [76].

The virtual array method is shortly described in the following. The corrected antenna pattern is calculated from

$$F_c(\theta) = \frac{1}{2}\left[F(\theta) + g\tilde{F}(\theta)\right], \tag{3.10}$$

where $F(\theta)$ is the antenna pattern measured in place, g is a complex phase factor and $\tilde{F}(\theta)$ is the antenna pattern measured in a displaced position. If the antenna is displaced in a transverse direction to the desired signal, the complex phase factor is $g = 1$, and the displacement is

$$d = \frac{\lambda}{2\sin\theta}, \tag{3.11}$$

where θ is the rotation angle of the antenna. If the antenna is displaced laterally, the displacement is

$$d = \frac{\lambda}{2(\cos\theta - 1)}, \tag{3.12}$$

and the complex phase factor is

$$g = e^{-jkd}, \tag{3.13}$$

where k is the wave number. The optimal displacement direction depends on the angular range of the antenna pattern which is being corrected. If the antenna pattern is corrected at small angles, i.e., close to the main beam, lateral displacement is more desirable. If the antenna pattern is corrected at large angles, transverse displacement is more attractive. The method has been demonstrated at 16 GHz.

3.3.3 Novel Antenna Pattern Comparison

In the novel antenna pattern comparison (NAPC) the complex antenna pattern (both amplitude and phase) of the antenna under test is measured several times at different known locations. The corrected pattern is obtained from the measured patterns using a circle fitting algorithm [77]. In this technique, it is assumed that in each point the received signal is a vector sum of the direct signal and the reflected spurious signal, as shown in Figure 3.3. The received vectors at each measurement positions are normalized so, that the direct signal components are in-phase, as shown in Figure 3.4.

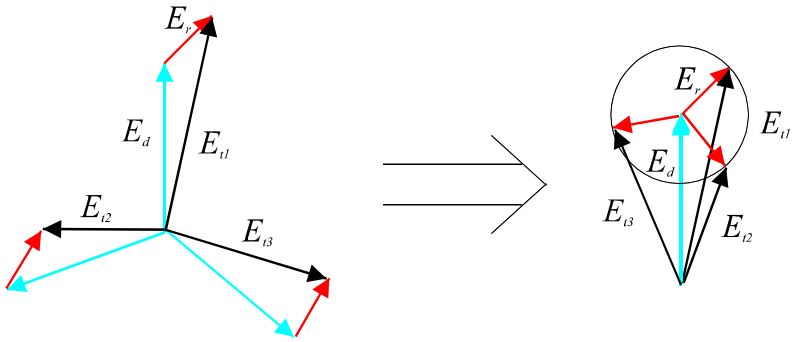

Fig. 3.4. The received signals are phased in the NAPC method so, that the direct signal components are in-phase.

These normalized vectors span a circle, whose radius equals to the amplitude of the spurious signal and the center equals to the amplitude of the direct signal. Let us consider phase normalized measurement results $P_{meas,i}$ at one antenna rotation angle θ_n plotted on a complex plane over different measurement locations, as shown in Figure 3.5.

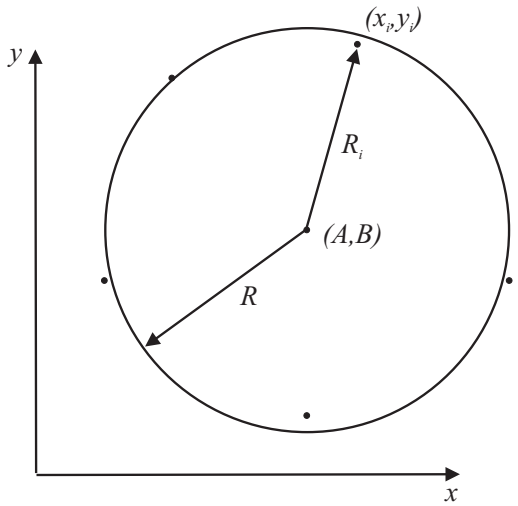

Fig. 3.5. Phase normalized measurement results at one antenna rotation angle plotted over different measurement locations.

The coordinates x_i and y_i are defined as:

$$\begin{aligned} x_i &= real\{P_{meas,i}(\theta_n)\} \\ y_i &= imag\{P_{meas,i}(\theta_n)\}. \end{aligned} \tag{3.14}$$

In the NAPC method, a circle satisfying the following modified least squares error criterion, is fitted to the measurement results [78]:

$$\sum_{i=1}^{N}\left(R_i^2 - R^2\right)^2 = \min . \tag{3.15}$$

The circle parameters A, B, and R are solved from [78]

$$\begin{pmatrix} A \\ B \\ R^2 - A^2 - B^2 \end{pmatrix} = \mathbf{D}^{-1}\mathbf{E}, \tag{3.16}$$

where

$$\mathbf{D} = \begin{pmatrix} 2\sum_i x_i & 2\sum_i y_i & N \\ 2\sum_i x_i^2 & 2\sum_i x_i y_i & \sum_i x_i \\ 2\sum_i x_i y_i & 2\sum_i y_i^2 & \sum_i y_i \end{pmatrix}, \tag{3.17}$$

and

$$\mathbf{E} = \begin{pmatrix} \sum_i \left(x_i^2 + y_i^2\right) \\ \sum_i \left(x_i^3 + x_i y_i^2\right) \\ \sum_i \left(x_i^2 y_i + y_i^3\right) \end{pmatrix}. \tag{3.18}$$

Practical issues on circle fitting in the NAPC method are discussed in [79]. The NAPC has been demonstrated with a 1.85-m diameter reflector antenna at 11.95 GHz [80] and with 2-m reflector antenna at 11.5 GHz [77].

3.3.4 Adaptive Array Correction Strategy

The adaptive array correction strategy employs similar data as the NAPC. In this method, the MUSIC algorithm is used at each antenna pointing angle to find the directions of the spurious signals. Then an array is formed, that has nulls towards spurious signals and high directivity toward the direct signal [81]. The method is shortly described in the following.

Let us consider a linear array of M equispaced isotropic elements. The received signal at the ith element consists of $K < M$ plane waves and noise n_i as:

$$x_i = \sum_{k=1}^{K} a_k e^{j((i-1)2\pi d \sin(\theta_k)/\lambda + \psi_k)} + n_i \,, \tag{3.19}$$

where θ_k is the direction-of-arrival of the *k*th plane wave, a_k is the amplitude of the *k*th plane wave, ψ_k is the phase of the *k*th plane wave, and d is the interelement distance.

All signals in an antenna test range usually derive from the range feed and therefore the signals are correlated. The superresolution techniques assume uncorrelated signals and therefore the measured signals are numerically uncorrelated by using a spatial smoothing. The smoothing is done by dividing the array of M elements into overlapping subarrays of L $(L < K, P \geq K)$ elements [82]. The output data are arranged as:

$$\mathbf{X} = \begin{bmatrix} \sqrt{g_1}x_1 & \sqrt{g_2}x_2 & \cdots & \sqrt{g_P}x_P \\ \sqrt{g_1}x_2 & \sqrt{g_2}x_3 & \cdots & \sqrt{g_P}x_{P+1} \\ \cdots & \cdots & \cdots & \cdots \\ \sqrt{g_1}x_L & \sqrt{g_2}x_{L+1} & \cdots & \sqrt{g_P}x_{P+L} \end{bmatrix}, \tag{3.20}$$

where g_p are real weighting constants. The singular value decomposition of $\mathbf{X}$ is

$$\mathbf{X} = \mathbf{U}\Sigma\mathbf{V}^* , \tag{3.21}$$

where $\mathbf{U} = [\mathbf{u}_1, \mathbf{u}_2, ..., \mathbf{u}_L]$ is a matrix whose columns are the left singular vectors of the matrix $\mathbf{X}$, $\mathbf{V} = [\mathbf{v}_1, \mathbf{v}_2, ..., \mathbf{v}_L]$ is a matrix whose columns are the right singular vectors, * denotes the conjugate transpose, and Σ is a diagonal matrix containing the singular values of $\mathbf{X}$ in ascending order. The noise subspace of $\mathbf{X}$ is given as $\mathbf{E}_N = [\mathbf{u}_{K+1}, \mathbf{u}_{K+2}, ..., \mathbf{u}_L]$, and the angular spectrum of the signals are estimated with

$$H(\theta) = \frac{\mathbf{a}^*(\theta)\mathbf{a}(\theta)}{\mathbf{a}^*(\theta)\mathbf{E}_N\mathbf{E}_N^*\mathbf{a}(\theta)} , \tag{3.22}$$

where $\mathbf{a}(\theta) = [1, e^{j2\pi d \sin(\theta)/\lambda}, e^{2j2\pi d \sin(\theta)/\lambda}, ..., e^{(L-1)j2\pi d \sin(\theta)/\lambda}]$ is the steering vector. The direction-of-arrival of the signals are indicated by the peaks of the $H(\theta)$.

For filtering the interference signals out, it is required that

$$\mathbf{H}^*\mathbf{w} = 0 \,, \tag{3.23}$$

where $\mathbf{H} = [\mathbf{a}(\theta_2), \mathbf{a}(\theta_3), ..., \mathbf{a}(\theta_K)]$ and $\mathbf{w}$ is the weighting vector of the array. The right singular vectors associated to singular values of the $\mathbf{H}^*$ having zero value ($\mathbf{v}_K, \mathbf{v}_{K+1}, ..., \mathbf{v}_M$) form the nullspace of $\mathbf{H}^*$. The vectors are grouped as $\mathbf{T} = (\mathbf{v}_K, \mathbf{v}_{K+1}, ..., \mathbf{v}_M)$ and therefore $(\mathbf{Ty})^* \mathbf{a}(\theta) = 0$ in $\theta = \theta_2, \theta_3, ..., \theta_K$ for any vector $\mathbf{y}$. The element giving maximum directivity in the direction of the desired signal is chosen by solving

$$\max_{y} \frac{(\mathbf{Ty})^{*}\mathbf{a}(\theta_1)\mathbf{a}^{*}(\theta_1)\mathbf{Ty}}{(\mathbf{Ty})^{*}\mathbf{BTy}}, \tag{3.24}$$

where $\mathbf{B} = 1/4\pi \int_{4\pi} \mathbf{a}(\theta)\mathbf{a}^{*}(\theta)d\theta$. Finally the weights are normalized such, that the directivity of the array remains constant to the desired signal direction. The method has been demonstrated at the X-band (8 – 12 GHz).

3.4 Discussion on Antenna Pattern Correction Techniques

The techniques employing the measured quiet-zone field do not seem practical at submillimeter wavelengths due to their challenging implementation. There are available no large reference antennas that could be used in the deconvolution. The quiet-zone field probing is possible with a near-field scanner, but it is still as challenging as a complete near-field measurement of the AUT, and therefore it would be practical to perform the near-field measurement alone. A quiet-zone field probing on a sphere enclosing the antenna under test seems to be very challenging or even impossible at submillimeter wavelengths.

Most of the time and frequency techniques seem practical at submillimeter wavelengths. Only a possibility to change the frequency is needed. The frequency shift technique is the simplest, in which the antenna pattern measurement needs to be performed at least at two different frequencies. Other more sophisticated techniques require that the frequency can be swept. The measurement time with these methods does not increase significantly if different frequencies can be measured fast with a network analyzer. In addition, the spatial resolution (and the correction accuracy) of these techniques depends on the bandwidth. Even large bandwidths are relatively small at submillimeter wavelengths as compared to that of microwave frequencies.

Implementing of the hard gating may be problematic, as a fast RF switch is needed. Implementing of the channel equalization method requires a possibility to modulate the signal. This may be problematic at submillimeter wavelengths.

The APC method seems as a suitable correction technique at submillimeter wavelengths. The method is relatively simple to implement. Only a translation stage is needed for moving the combination of the antenna under test and the antenna rotation stage. Other spatial techniques require more sophisticated translation stage. In the NAPC and adaptive array strategy the position of the AUT need to be known accurately (with an accuracy of approximately $\lambda/100$). The most sophisticated antenna positioner is required when implementing the virtual array method. The antenna positioner must be able to displace the antenna as a function of the rotation angle. At submillimeter wavelengths this method does not seem practical. The submillimeter wave antennas are potentially very heavy and the displacement accuracy requirement is high because of the small wavelength. However, the NAPC and the adaptive array strategy seem realizable, because the antenna translation stage does not need to be accurate. Only the position of the AUT needs to be measured accurately. This could be done with a laser interferometer, for example.

The adaptive array strategy is potentially sensitive to interference signals originating from the near-field of the array, as the MUSIC algorithm is used for detecting the interference signals. The far-field conditions can be assumed in antenna ranges at microwave frequencies, but they are not likely satisfied at submillimeter wavelengths. The NAPC suffers from the near-field

conditions as well. As the amplitude of the spurious signal is not constant, the received signals do not span a circle when plotted over several positions.

The drawback with the spatial techniques as compared to time or frequency techniques is that the measurement time is increased significantly, because a mechanical movement is required instead of sweeping the frequency.

3.5 Stray Signal Imaging

A test-zone field of a far-field or a compact range is generally probed in order to verify that the field meets certain specifications. In addition to the field verification, this probe data can be used to image stray signals in the range. After the stray signals are located, the range can be modified to remove the stray signals and the measurement procedure can be designed to minimize the effects of the stray signals.

Most of the techniques are developed for microwave frequencies and they are not directly suitable at submillimeter wavelengths. For example, far-field (i.e. plane wave) conditions are assumed in all direction-of-arrival techniques. Most of the techniques are reviewed in [83].

3.5.1 Direction-of-Arrival Techniques

In the direction-of-arrival (DOA) techniques, the plane wave spectrum is calculated from the field probe data. The highest peak in the plane wave spectrum represents the desired planar wave front whereas other peaks are caused by spurious signals. The scatterers are then located according to the directions of the spurious signals in the plane wave spectrum.

The plane wave spectrum can be obtained with the Fourier transform or with superresolution techniques [84], [85], such as MUSIC (Multiple Signal Classification) [86]. The Fourier-transform technique is simpler and more robust than the superresolution techniques, but it may have lower angular resolution and worse detection of the spurious signals. Superresolution techniques assume that all signals are uncorrelated with each other. Usually all spurious signals are originated from the range transmitter, and therefore all signals are correlated. This problem can be mitigated by using a pre-whitening procedure, in which the correlated signals are numerically uncorrelated [84]. This is done with a cost of decreased angular resolution.

Direction-of-arrival techniques assume plane wave conditions, i.e., the scatterers are in the far-field of the test-zone scanner. At high frequencies this condition is usually not met. For example, the far field distance for a 1 m scanning area at 300 GHz is 2 kilometers. Especially superresolution techniques can handle poorly these non-idealities. To avoid these problems, the field probe data can be divided into smaller areas so that the far-field condition is satisfied.

In the papers [P6] and [5], a practical exploitation of the Fourier-transform method for stray signal imaging at submillimeter wavelengths is described. The papers describe a measurement campaign of a 1.5 meter antenna at 322 GHz in a hologram-based CATR. The quiet-zone field was probed with a plane-polar scanner prior to antenna tests. The plane wave spectrum, which was calculated from the measured quiet-zone field, indicated a stray signal arriving approximately from the direction of 8° in the horizontal plane. The effect of the stray signal was also found in the antenna pattern measurements.

3.5.2 Near-Field Focusing

In the near-field focusing, the phase of the measured data is adjusted to focus the measured field at a given point in the image domain [83]. The maxima in the image domain represent the scatterers. The near-field focusing is able to locate sources which scatter a spherical wave front. Because the quiet-zone field is mainly planar, it does not focus at a single spot, and thus the image caused by the planar wave front may conceal weak scattering objects. The near-field focusing technique may be improved by subtracting the planar wave front from the probed field data. Planar wave front subtraction techniques are discussed in Section 3.5.3. The near-field focusing might be a suitable technique at submillimeter wavelengths as the far-field condition is not assumed.

3.5.3 Planar Wavefront Estimation

In the direction-of-arrival techniques, the finite length of the probe data causes side lobes to the plane wave spectrum. These side lobes may conceal weak stray signals. Also the near-field focusing suffers from the presence of a strong direct signal. Several techniques have been introduced for improving the performance of the stray signal imaging techniques by subtracting the direct signal from the field probe data. The direct signal can be cancelled from the field probe data for example by using a probe with a null in the broadside direction or applying numerical spatial filters [87]. One possibility is to measure the field probe data on two planes with half a wavelength separation. As the data on both planes are added point wise, the direct signal component is cancelled out [88].

3.5.4 Techniques in Time Domain

Stray signal information in the time domain is useful if the path length of the stray signal differs from the path length of the direct signal. In such a case, the stray signals can be imaged due to their different times-of-arrival. If the time domain response is calculated for each probe position, the signals received at each probe position can be identified. Another possibility is to use the direction-of-arrival estimation or near-field focusing in time domain.

The time domain data can be obtained if the field probe data is recorded over a certain frequency band. When sweeping the frequency, the equipment should be calibrated in order to separate the frequency response of the equipment from the frequency response of the test range. A technique to calibrate the field probe data for the equipment using the desired planar wave front is introduced in [89].

4 Correction Techniques Developed in the Thesis

This Chapter presents four antenna pattern correction techniques that have been developed in this thesis. The techniques are the feed scanning based antenna pattern comparison, the frequency shift method for hologram-based CATRs, the adaptive array method, and the method for maximizing the signal-to-interference ratio. Each of these techniques is first briefly introduced and then the experimental and numerical methods for verifying these techniques are described.

4.1 Frequency Shift Method for Hologram-Based CATRs

The frequency shift technique (Section 3.2.1) was already introduced in the early era of anechoic chambers. At that time the method was used at low microwave frequencies, and it was not seen attractive due to its large relative bandwidth requirements. However, it is shown in [P3] and [9] that the method has high potential at submillimeter wavelengths, where the required bandwidth is relatively small. It is also shown in [P3] that the method has a great advantage in the hologram-based compact antenna test ranges. The method is able to partially compensate possible non-ideal operation of the hologram.

4.1.1 Principle of the Frequency Shift Technique in a Hologram-Based CATR

As a hologram is a dispersive element, its non-ideal operation, such as edge diffraction can be partially corrected with the frequency shift method. Let us consider a hologram-based CATR in Figure 4.1.

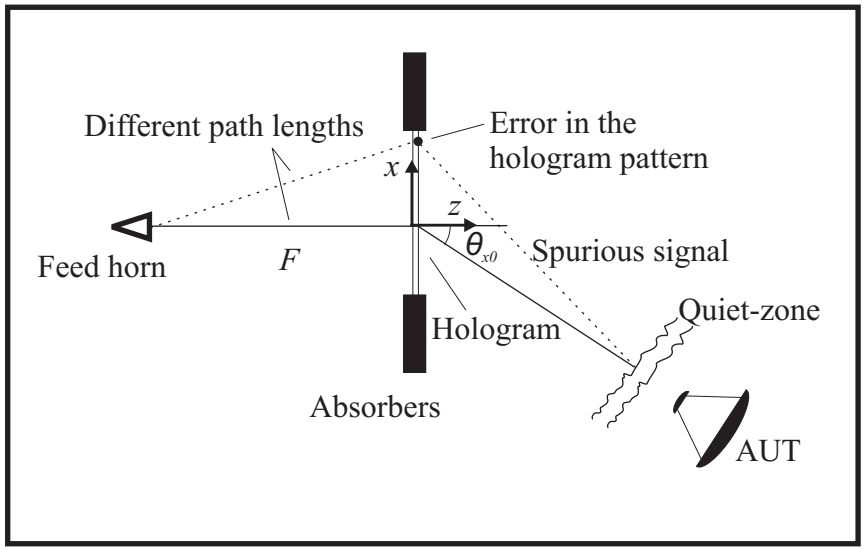

Fig. 4.1. A hologram-based CATR with a disturbance in the hologram pattern.

There is a disturbance in the edge of the hologram pattern, which causes a spurious signal to the quiet-zone. As the hologram is a planar structure, the signal path length to the edge of the hologram is longer than that to the center of the hologram. Therefore the phases of the direct and spurious signals change differently with the frequency. This enables partial correction of the disturbances caused by the hologram.

4.1.2 Bandwidth Limitations

A hologram is a dispersive element and therefore its bandwidth limitations need to be taken into account. The bandwidth of the hologram depends on the required quiet-zone field quality. By requiring the general far-field criterion (2.1), the relative bandwidth of the hologram can be calculated from

$$\frac{\Delta f}{f_0} = \pm \frac{\lambda_0}{16\left(\sqrt{F^2 + (D/2)^2} - F\right)}, \tag{4.1}$$

where λ_0 is the wavelength at the center frequency, F is the focal length of the hologram and D is the diameter of the antenna under test. Changing the frequency also steers the direction of the plane wave produced by the hologram. The steered direction is given as

$$\theta = \arcsin\left(\frac{\lambda}{\lambda_0}\sin\theta_{x0}\right), \tag{4.2}$$

where θ_{x0} is the original direction of the plane wave. The steering of the plane wave is usually so small, that it does not need to be considered.

The bandwidth of the AUT should also be taken into account. Hologram CATRs are generally used to measure very broad band antennas, such as reflector or lens antennas. In these antennas, only the electrical size of the aperture changes with the frequency (assuming no multiple reflections inside the antenna). Therefore the antenna pattern of such an antenna is only scaled in the angular domain as a function of the frequency. The maximum shift in the antenna pattern should be much smaller than the width of a side lobe

$$\frac{\Delta\lambda}{\lambda_0}\alpha_{max} << \frac{\lambda_0}{D}, \tag{4.3}$$

where $\Delta\lambda$ is the change of the wavelength and α_{max} is the maximum angle of the antenna pattern, where the correction is performed. For example, the angular shift at 10º is 15 % of the width of the side lobe, if the original frequency of 310 GHz is shifted 3.5 GHz and the antenna diameter is 76.2 mm.

4.1.3 Correction Efficiency

The correction efficiency of the frequency shift method depends on the used bandwidth. On the other hand, the bandwidth is usually limited by the hologram, and it is given in (4.1). The relative bandwidth of the hologram depends on the range geometry, the size of the AUT, and the center frequency. Usually it is possible to fully correct the effects of the spurious signals originating from the edges of the hologram and to partially correct the effects of the spurious signals originating closer from the hologram center.

4.2 Feed Scanning Based APC

As concluded in Section 3.4, the antenna pattern comparison is a potential antenna pattern correction technique at submillimeter wavelengths. When implementing the APC technique, there must be a possibility to move the combination of the antenna rotation stage and the

antenna under test. This may be challenging since high-gain submillimeter antennas are potentially extremely heavy. In the feed scanning APC, the light weight transmitter of a CATR is moved instead of the AUT. The feed scanning APC is first introduced in [10] and [P4]. The technique is also adopted in a commercial compact range [90].

4.2.1 Principle of the Method

It is assumed in the feed scanning APC that all the spurious signals originate from the range feed antenna, i.e., no external signal sources are present. It is also assumed that the path length of the spurious signal differs from the path length of the straight signal. In that case, it is possible to cause a phase difference to the spurious signal by moving the transmitter. The principle of the method is presented in Figure 4.2.

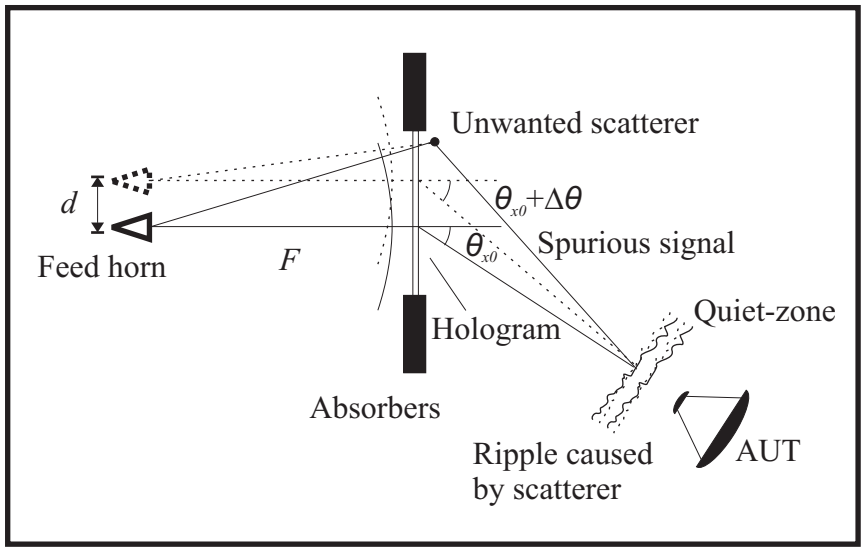

Fig. 4.2. Different phase change of the desired plane wave and spurious signal in the feed scanning based APC method. In this figure the CATR collimating element is a hologram, but the same principle applies also in case of a reflector as the collimating element.

In the feed scanning APC, the antenna pattern of the AUT is measured several times with different transmitter positions. As the path length of the spurious signal differs from the path length of the desired signal, the relative phase difference between the desired plane wave and spurious signal is different at each feed position. The effect of the spurious signal is compensated and the corrected pattern is obtained by averaging the measured patterns.

This principle can be used to compensate the errors caused by standing waves between the transmitter and collimating element as well as errors caused by other spurious signals. The emphasis of this study is on the compensation of the errors caused by spurious signals other than the multiple reflections.

4.2.2 Optimal Feed Displacement Interval and Range

The angular range of the AUT, Ψ_{AUT}, in which the correction is performed, is first decided. The angular range is then projected to the feed via range walls and objects, in order to define the most harmful directions of the scatterers seen from the feed antenna (Figure 4.3).

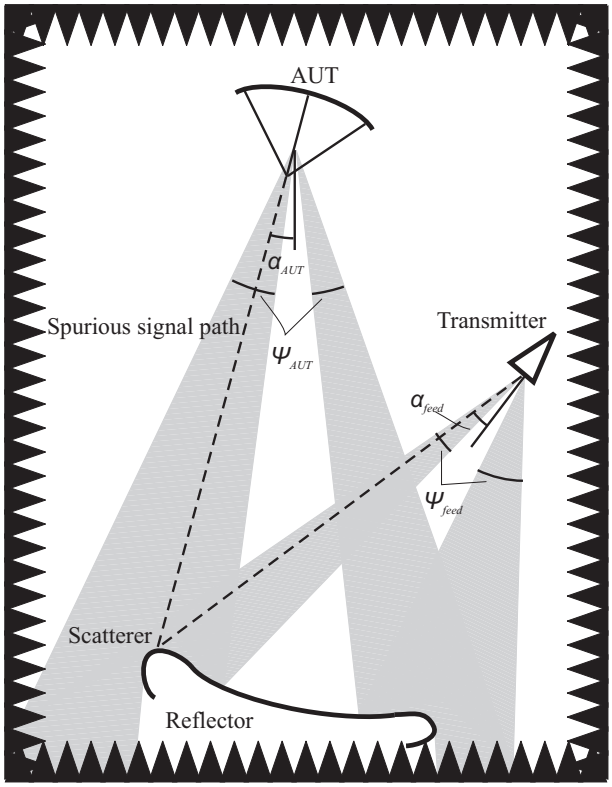

Fig. 4.3. The angular range of the antenna pattern, where the correction is performed, is projected to the transmitter. The optimal feed displacements are calculated from the projected range.

The optimal feed displacements are calculated from the angular range reflected to the feed Ψ_{feed}. The transversal interference period d of two plane waves is

$$d = \frac{\lambda}{\sin\varphi}, \tag{4.4}$$

where λ is the wavelength and φ is the angle between the plane waves. In this case the angle φ is the angle projected to the feed antenna. Basically, the largest angle ($\max|\Psi_{feed}|$) defines the displacement interval and the smallest angle ($\min|\Psi_{feed}|$) defines the displacement range. According to the Nyquist sampling theorem, the displacement interval should be less than one half of the smallest interference period. The displacement range depends on how many periods one wants to capture. Theoretically one period is enough to compensate the effect of the spurious signal. The displacement interval can be calculated from

$$d_{int} = \frac{\lambda}{2\sin(\max|\Psi_{feed}|)}. \tag{4.5}$$

Similarly, the displacement range can be calculated from

$$d_{range} = \frac{\lambda}{\sin(\min|\Psi_{feed}|)}. \tag{4.6}$$

The required number of the measurements can be calculated from (4.5) and (4.6). Basically, the wider is the angular range to be corrected the more measurements are needed. The critical factor here is usually the minimum of the angular range. When the correction is performed at small angles, the required displacement range may be huge. However, the correction range does not need to cover the main beam, because the effect of the stray signals on the main beam measurement is small.

4.2.3 Limitations to the Feed Displacement

When the feed is displaced from the focus of the collimating element, certain things need to be considered. First of all, moving the feed transversally steers the plane wave produced by the collimating element. The steered direction can be calculated from

$$\Delta\theta \approx \frac{d}{F\cos\theta_{x0}}, \tag{4.7}$$

where d is the feed displacement, F is the focal length of the collimating element and θ_{x0} is the original direction of the plane wave (Figure 4.2). The whole aperture of the AUT should remain in the quiet-zone when the feed is displaced.

The feed displacement also changes the phase and the amplitude of the quiet-zone field. The phase variation from the linear phase slope behind the hologram caused by moving the feed can be calculated from

$$\Delta\phi = \frac{2\pi}{\lambda}\left(\sqrt{F^2+(d+x)^2} - \sqrt{F^2+x^2} - \frac{dx}{F}\right), \tag{4.8}$$

where x is the coordinate on the hologram surface and λ is the wavelength. The general criterion for the quiet-zone phase ($\pm 5°$) should be fulfilled on the aperture of the AUT. Transversal movement of the feed changes also the hologram illumination. This results in a quiet-zone field with a slope in the amplitude. However, the change in the illumination can be mostly compensated by redirecting the feed towards the hologram (or reflector) center. Usually, this is not needed as the displacements are so small that the illumination remains practically unchanged.

4.3 Adaptive Array Based Correction Technique

In the adaptive array based pattern correction technique [P5], [11] the antenna pattern of the AUT is measured at several accurately known locations in the quiet-zone, as is done also in virtual array, NAPC, and adaptive array strategy presented in Chapter 3. The advantage of the adaptive array based technique over the previously developed techniques is that it potentially is not as sensitive to the far-field criterion, which is not usually met when measuring highly directive antennas.

The adaptive array based correction technique is an iterative technique, which suits for compact and far-field ranges. The method fits best for measuring directive antennas, but it can be easily modified for measuring antennas with low directivity also.

4.3.1 Principle of the Method

The antenna pattern measurements performed at different locations form a virtual antenna array at each rotation angle of the AUT, as shown in Fig. 4.4.

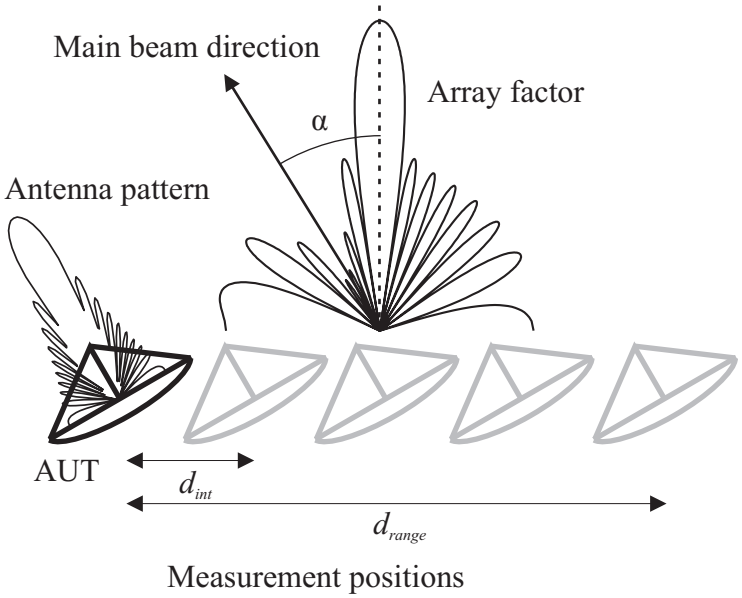

Fig. 4.4. A virtual array is formed when the antenna pattern of the AUT is measured at several locations in the quiet-zone. The figure is not to scale.

The array pattern (the antenna pattern of the virtual array) at the AUT rotation angle of α can be calculated from

$$P_{AP}(\theta) = P_{AF}(\theta) P_{AUT}(\theta - \alpha), \tag{4.9}$$

where P_{AF} is the array factor and P_{AUT} is the antenna pattern of the AUT. In this method, the array factor is modulated at each antenna rotation angle such, that the array pattern has high directivity towards to desired signal arriving from the direction of $0°$ and high attenuation to other directions.

4.3.2 Measurement Positions

The angular range of the antenna pattern, in which the correction can be performed, depends on the measurement positions (or element locations of the array). For simplicity, only uniformly spaced measurement positions are considered here. The smallest angle, in which the correction can be performed depends on the displacement range d_{range} whereas the largest angle depends on the displacement interval d_{int}. The first null of the uniformly weighted array (with isotropic elements) occurs at

$$\theta_{min} = \arcsin \frac{\lambda}{d_{range}} \approx \frac{\lambda}{d_{range}}, \tag{4.10}$$

which is approximately the smallest angle in which the correction can be performed. If the displacement interval does not satisfy the fundamental sampling criterion of $\lambda/2$, the array factor has higher order grating lobes in the directions of

$$\theta_{max} = \arcsin\frac{n\lambda}{d_{int}}, \quad n = \pm 1,2,3,... \tag{4.11}$$

The correction is not possible in these directions.

4.3.3 Array Synthesis

The array factors are synthesized by using the alternating projections method [91], [92]. The implementation described in [91] is based on Fourier-transform whereas the implementation described in [92] is based on matrix-inversion. The matrix-inversion approach is described in the following.

A mask, i.e. the upper and lower limits M_u and M_l, for the synthesized amplitude pattern of the array is first defined in the synthesis. The procedure for defining the mask is discussed later. The iteration begins from the initial guess for the element weights $\mathbf{w}_0$. The corresponding array pattern is calculated with

$$\begin{bmatrix} P_{ap}(\mathbf{u}_{r,1}) \\ P_{ap}(\mathbf{u}_{r,2}) \\ \vdots \end{bmatrix} = \begin{bmatrix} g(\mathbf{u}_{r,1})e^{jk\mathbf{r}_1\cdot\mathbf{u}_{r,1}} & g(\mathbf{u}_{r,1})e^{jk\mathbf{r}_2\cdot\mathbf{u}_{r,1}} & \cdots \\ g(\mathbf{u}_{r,2})e^{jk\mathbf{r}_1\cdot\mathbf{u}_{r,2}} & g(\mathbf{u}_{r,2})e^{jk\mathbf{r}_2\cdot\mathbf{u}_{r,2}} & \cdots \\ \vdots & \vdots & \ddots \end{bmatrix} \begin{bmatrix} w_1 \\ w_2 \\ \vdots \end{bmatrix}, \tag{4.12}$$

or

$$\mathbf{P}_{AP} = \mathbf{G}\mathbf{w}, \tag{4.13}$$

where $\mathbf{G}$ is the array response matrix, g is the element pattern, k is the wave number, $\mathbf{u}_r$ is the unit direction vector, and $\mathbf{r}$ is the location vector. The element pattern is not known, but it is estimated as a uniform average of the measured patterns:

$$g(\mathbf{u}_r) \approx \frac{1}{N}\sum_{n=1}^{N} P_{AUT,n}(\mathbf{u}_r), \tag{4.14}$$

where $P_{AUT,n}$ is the nth measured antenna pattern. A projector operator $\mathcal{P}$ is then applied to the array pattern. The projector operator conserves the array pattern at the angles, in which the array pattern is within the mask, and replaces the array pattern with the limit values at angles, in which the array pattern exceed the limit values as

$$\mathcal{P}P_{AP}(\mathbf{u}_r) = \begin{cases} M_u(\mathbf{u}_r), & |P_{AP}(\mathbf{u}_r)| > M_u(\mathbf{u}_r) \\ P_{AP}(\mathbf{u}_r), & M_l(\mathbf{u}_r) \le |P_{AP}(\mathbf{u}_r)| \le M_u(\mathbf{u}_r). \\ M_l(\mathbf{u}_r), & |P_{AP}(\mathbf{u}_r)| < M_l(\mathbf{u}_r) \end{cases} \tag{4.15}$$

The limited array pattern is transformed back to the element weights by using pseudo-inverse of the array response matrix. The iteration formula for the array weights is

$$\mathbf{w}_{n+1} = \left(\mathbf{G}^{*}\mathbf{G}\right)^{-1}\mathbf{G}^{*}\mathcal{P}\mathbf{G}\mathbf{w}_{n}, \tag{4.16}$$

where * denotes complex conjugate transpose. The iteration is repeated a prescribed number of cycles or until a certain stopping criterion is fulfilled.

4.3.4 Mask for the Synthesized Array Pattern

The realizable limits for the array pattern depend on the antenna pattern of the AUT, the measurement positions of the AUT, and the number of the measurements. Therefore there is no simple rule for defining the limits, but the user should iteratively try what limits are realizable. The angular interference spectrum can be taken into account when defining the limits: More attenuation is applied to the directions of high interference than to the directions of low interference. The interference spectrum can be estimated from the measured antenna patterns for example as

$$p(\mathbf{u}_r) = \max_n \left| \frac{1}{N}\sum_{n=1}^{N} P_{AUT,n}(\mathbf{u}_r) - P_{AUT,n}(\mathbf{u}_r) \right|^2 . \tag{4.17}$$

Equation (4.17) assumes that the deviations between the measured antenna patterns are caused by an interference signal arriving through the main beam. Therefore (4.17) holds best with highly directive antennas.

4.4 Technique for Optimizing the Signal-to-Interference Ratio

The technique for optimizing the signal-to-interference ratio employ antenna patterns measured at several accurately known positions in the quiet-zone [P6]. As the adaptive array technique, also this technique tolerates well spurious signals arriving from the near-field region. The advantage with this method over the adaptive array based method is an analytical solution, which theoretically provides better accuracy. The applicability of this method is similar to that of the adaptive array based technique: it suits best for measuring highly directive antennas in compact and far-field ranges, but it can be easily modified for measuring also antennas with low directivity.

4.4.1 Theory

Let us consider an antenna pattern measurement, which is repeated N times at different locations, as shown in Figure 4.5.

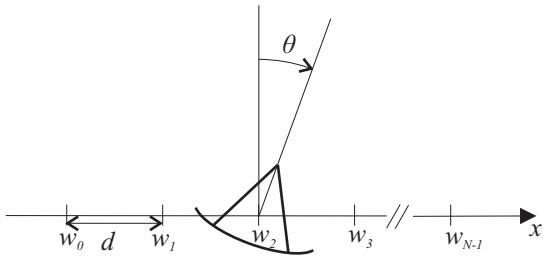

Fig. 4.5. The antenna pattern measurement is repeated N times at different locations.

Assume that the angular interference power spectrum is given by $p(\theta)$, and that the desired plane wave arrives from the direction of $\theta = 0$. The measurement positions are weighted with

complex weights w_n and they form a virtual antenna array, whose array factor can be calculated from

$$P_{AF}(\theta) = \sum_{n=0}^{N-1} w_n e^{jnkd\sin\theta} . \tag{4.18}$$

The array pattern of the array at the antenna rotation angle of α is given as

$$P_{AP}(\theta) = P_{AF}(\theta) P_{AUT}(\theta - \alpha), \tag{4.19}$$

where P_{AUT} is the antenna pattern of the AUT. The interference power received by the antenna array at the antenna rotation angle of α is

$$\begin{aligned} I &= \int_{-\pi}^{\pi} |P_{AP}(\theta)|^2 p(\theta) kd\cos\theta d\theta \\ &= \int_{-\pi}^{\pi} |P_{AF}(\theta)|^2 |P_{AUT}(\theta - \alpha)|^2 p(\theta) kd\cos\theta d\theta \end{aligned}, \tag{4.20}$$

which can be written as

$$I = \int_{-\pi}^{\pi} |P_{AF}(\theta)|^2 p_{ef}(\theta, \alpha) kd\cos\theta d\theta , \tag{4.21}$$

where $p_{ef}(\theta, \alpha)$ denotes the angular interference spectrum weighted with the shifted antenna pattern of the AUT. Let us define the spatial correlation coefficients for $p_{ef}(\theta, \alpha)$ as

$$H_l(\alpha) = \frac{1}{2\pi} \int_{-\pi}^{\pi} p_{ef}(\theta, \alpha) e^{jlkd\sin\theta} kd\cos\theta d\theta . \tag{4.22}$$

It is shown in [93], that the signal-to-interference ratio is maximized when the complex element weights w_n satisfy

$$\sum_{m=0}^{N-1} H_{n-m} w_m = 1 . \tag{4.23}$$

4.4.2 Method

Both the angular interference power spectrum and the antenna pattern of the AUT are first estimated from the measured antenna patterns and then a more accurate estimate for the antenna pattern of the AUT is obtained using these first-order estimates. The antenna pattern of the AUT and the interference power spectrum are estimated using (4.14) and (4.17), respectively. The spatial correlation coefficients are then solved from (4.22) and the optimal weights from (4.23). The corrected antenna pattern is finally obtained from

$$P_{COR}(\alpha) = \sum_{n=0}^{N-1} w_n(\alpha) P_{AUT,n}(\alpha). \tag{4.24}$$

4.5 Verification of the Methods

The correction techniques developed in this thesis have been verified both with physical test antennas experimentally and with synthetic test antennas numerically. The tests with the physical test antenna verify the methods in a real environment. However, the antenna pattern of the physical test antenna is not exactly known, and therefore the correction accuracies of the methods can not be investigated. Because the antenna patterns of the synthetic test antennas are known, the accuracies provided by the methods can be compared with numerical simulations. The accuracies provided by each method are compared to that provided by the conventional APC.

4.5.1 Experimental Verification of the Methods

The methods are verified in a hologram-based CATR at 310 GHz. The focal length of the hologram is 1.8 m and the hologram diameter is 0.6 m. The hologram is illuminated with a corrugated horn. The transmitter is placed on a linear translation stage for optimizing the quiet-zone field and for moving the feed in the feed scanning APC. The hologram is a transmission-type amplitude hologram, which produces a plane wave propagating to an angle of 33° from the normal of the hologram surface. The quiet-zone field is optimized at the distance of 1.8 m from the hologram. A planar near-field scanner is used to probe the quiet-zone field prior to antenna measurements and also for moving the antenna under test in antenna pattern correction techniques. A corrugated horn is used as a probe antenna and a vector network analyzer is employed in both the quiet-zone and antenna testing. The hologram operation is distorted for demonstration purposes by adding a vertical metal or plastic rods or strips behind the hologram. The hologram-based CATR is depicted in Figure 4.6.

a) b)

Fig. 4.6. A) CATR from the transmitter side. B) CATR from the receiver side.

Two test antennas are manufactured for testing the antenna pattern correction techniques. The feed scanning based APC is tested with a dielectric-loaded flat reflector antenna [7] (Figure 4.7). The antenna structure is based on two offset reflectors. The subreflector is flat and it is fed with a corrugated horn. The main reflector is also flat, but it is loaded with a dielectric lens, which operate as a collimator. The diameter of the antenna aperture is approximately 120 mm.

Fig. 4.7. Dielectric-loaded flat reflector antenna is used as a test antenna with the feed scanning APC technique.

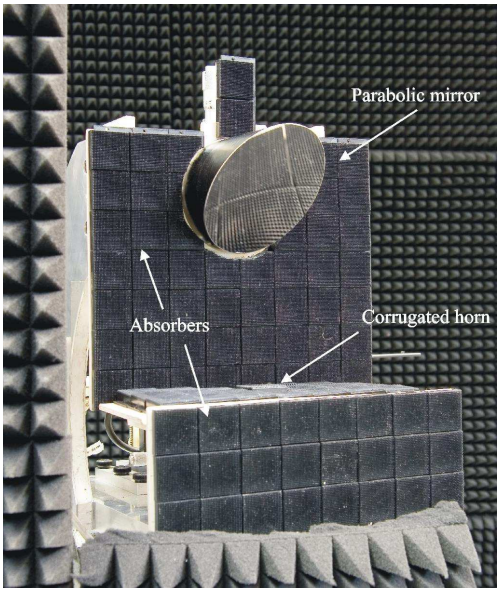

Fig. 4.8. The test antenna that is used in experimental verification of antenna pattern correction techniques.

Other techniques are verified with a different test antenna that is based on a single offset-fed parabolic mirror, see Figure 4.8. The reflector is a commercial optical component, which has high surface accuracy. The reflector diameter is 76.2 mm and its effective focal length is 127 mm. The offset angle is 90º and the feed is a corrugated horn. The beam of the horn is Gaussian with $-12\,\mathrm{dB}$ edge illumination in the plane of symmetry. Supporting structures are covered with radar absorbing material (RAM) in order to get good match with simulations and measurements. The antenna pattern of the test antenna is simulated with Grasp8W software.

4.5.2 Numerical Verification of the Methods

The numerical verification of the methods is based on the measured quiet-zone field E_{QZ} and on the simulated aperture distribution of a test antenna E_{AUT}. Let us consider the coordinate systems shown in Figure 4.9.

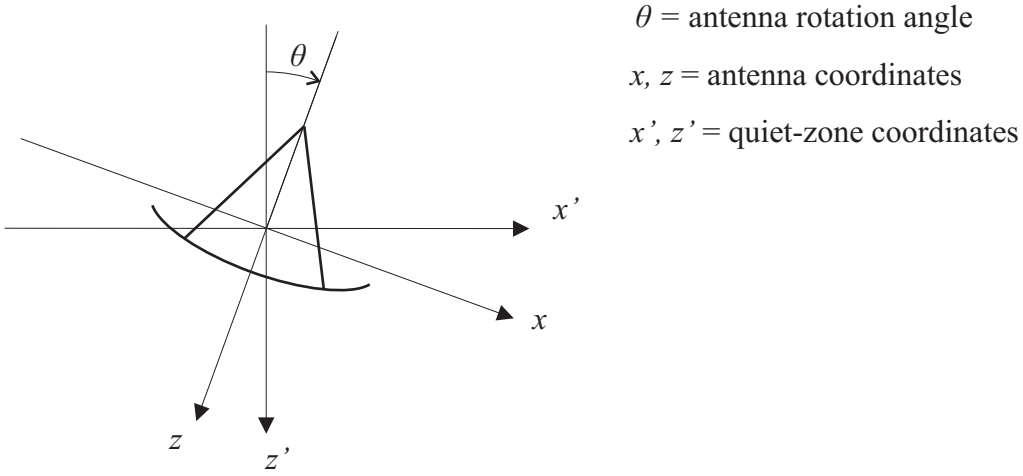

Fig. 4.9. The coordinate systems of the simulated test antenna and the quiet-zone.

The numerical verification is considered here only in two dimensions for simplicity, an extension to three dimensions being straightforward. The effect of the quiet-zone field to the measured antenna pattern of the AUT can be calculated from

$$P_{\mathrm{meas}}(k_x) = \int E_{QZ}(x) \cdot E_{AUT}(x) \cdot e^{-jk_k x} dx\,, \tag{4.25}$$

where $k_x = \dfrac{2\pi}{\lambda}\sin\theta$. The horizontal antenna coordinate x is given as

$$x = x'\cos\theta + z'\sin\theta\,. \tag{4.26}$$

By substituting (4.26) into (4.25) we get

$$P_{\mathrm{meas}}(k_x) = \int E_{QZ}(x'\cos\theta + z'\sin\theta) \cdot E_{AUT}(x) \cdot e^{-jk_k x} dx\,. \tag{4.27}$$

Equation (4.27) is problematic in practice, because it assumes that the quiet-zone field is measured in both coordinates x' and z'. If θ is small, the first order Taylor expansion of (4.27) is

$$P_{\text{meas}}(k_x) = \int E_{QZ}(x') \cdot E_{AUT}(x) \cdot e^{-jk_k x} dx \,. \tag{4.28}$$

Equation (4.28) is used in numerical verification for predicting the measured antenna pattern. The maximum angle of θ is 10° in numerical simulations, in which case the largest deviation between the x and x' is 1.5 percent.

The simulated test antenna that is used with the feed scanning based APC is circular with a diameter of 150 mm, and it has a Gaussian amplitude distribution with -12 dB edge illumination and flat phase. The simulated test antenna that is used with the other techniques is similar to the physical single offset-reflector test antenna. Both antennas are simulated with the Grasp8W program.

4.6 Results

The accuracies provided by the antenna pattern correction techniques developed in this thesis are compared to that provided by the conventional APC method. The accuracies of the feed scanning APC and the frequency shift method are found to be approximately equal to that provided by the APC. The accuracies provided by the adaptive array based technique and the signal-to-interference ratio optimization technique are much better than that: the errors in the corrected patterns obtained with these methods are even 30 dB lower than the errors in the corrected patterns obtained with the APC.

4.7 Summary of Publications

Paper [P1] presents the measurement results of a 1.5-m reflector antenna at 322 GHz. The measurements are carried out in a compact antenna test range that is based on a transmission-type amplitude hologram. Vertical and horizontal cuts of the antenna pattern are measured at co- and cross-polarizations and a contour map of the main beam region is measured at the co-polarization. The effect of the non-ideal quiet-zone field to the measured results is studied and the reasons for the deviations between the measurements and the simulations are discussed.

Paper [P2] reviews several antenna pattern correction techniques that have been developed for compact antenna test ranges or far-field ranges.

Paper [P3] points out the applicability of the frequency shift technique for hologram-based compact antenna test ranges. In the method, the antenna pattern of the antenna under test is measured several times at different frequencies. The applicability of the method is studied, and the method is verified in a hologram-based compact antenna test range at 310 GHz with measurements and simulations. The accuracy provided by the method is found to be approximately equal to that provided by the conventional APC.

Paper [P4] presents a new antenna pattern correction technique, which is suitable for compact antenna test ranges. In the technique, the antenna pattern of the antenna under test is measured several times using different range feed positions. The applicability of the method is studied, and the method is verified in a hologram-based compact antenna test range at 310 GHz with measurements and simulations. The accuracy provided by the method is found to be approximately equal to that provided by the conventional APC.

Paper [P5] presents a new antenna pattern correction technique, which is based on an adaptive array algorithm. The method is applicable for compact and far-field ranges. In the method, the

antenna pattern is measured several times at different locations in the quiet-zone. The method is verified in a hologram-based compact antenna test range at 310 GHz with measurements and simulations. The accuracy provided by the method is found to be better than that provided by the conventional APC.

Paper [P6] presents an improvement to the antenna pattern correction technique presented in [P5]. The proposed technique is based on maximization of the signal-to-interference ratio in the antenna pattern measurements. The method is verified in a hologram-based CATR with measurements and simulations. The accuracy provided by the method is found to be better than that provided by the conventional APC.

5 Conclusions

Several antenna pattern correction techniques have been previously developed for microwave frequencies for mitigating the effects of spurious signals and for increasing the measurement accuracy. Most of these methods are not directly applicable at submillimeter wavelengths and they have not been used in practical antenna tests at these frequencies.

In this thesis, four new antenna pattern correction techniques are developed: feed scanning APC technique, frequency shift technique, adaptive array based technique, and technique based on signal-to-interference ratio optimization. The applicability of each method is analytically studied and the methods are verified with measurements and simulations in a hologram-based CATR at 310 GHz. The feed scanning APC is as accurate as the conventional APC, but usually it is much more convenient to implement, as only a possibility to move the range feed antenna is needed. The feed scanning APC suits as well for all types of CATRs.

The frequency shift method, which has been originally developed for microwave frequencies, is found to be applicable at submillimeter wavelengths. The method suits for all CATRs. However, it offers a great advantage in the hologram-based CATRs. As the hologram is a dispersive element, the method is able to partially compensate possible non-ideal operation of the hologram. The correction accuracy of the frequency shift method is found to be approximately equal to that of the APC. Implementing the method is convenient as only a possibility to change the frequency is needed.

In the adaptive array correction technique and in the signal-to-interference ratio optimization technique the antenna pattern of the AUT is measured several times at different accurately known locations in the test range. In these methods, a virtual antenna array is formed from the measurement results at each rotation angle of the AUT. The array factor of the virtual array is then modulated such, that it has constant gain towards the desired signal and high attenuation to other directions. An estimate of the antenna pattern of the AUT and an estimate of the interference spectrum of the test range are used in the array synthesis. The adaptive array correction technique employs an alternating projections method in the array synthesis, whereas the other technique maximizes the signal-to-interference ratio. The accuracies of these techniques are found to be better than that of the conventional APC.

These antenna pattern correction techniques can be used to improve the measurement accuracy of CATRs and to push CATRs higher in frequency. In a nutshell, the following results obtained in this thesis work, advance the state-of-the-art of the antenna pattern correction techniques at submillimeter wavelengths:

1) A technique for maximizing the signal-to-interference ratio in the antenna pattern measurement, where the antenna under test is measured at several accurately known locations in the quiet-zone has been developed.

2) An adaptive array based antenna pattern correction technique has been developed for obtaining the corrected pattern from antenna patterns that are measured at different accurately known locations in the quiet-zone.

3) The applicability of the frequency shift method for the antenna pattern correction in hologram-based compact antenna test ranges has been demonstrated.

4) A feed scanning based antenna pattern comparison technique for the antenna pattern correction in compact antenna test ranges has been developed.

5) The effect of the realized quiet-zone field on the measured antenna pattern in a practical submillimeter wave antenna measurement has been estimated.

References

[1] T. Koskinen, V. Viikari, J. Häkli, A. Lönnqvist, J. Ala-Laurinaho, J. Mallat, and A.V. Räisänen, "A reflection-type amplitude hologram as a collimating element in compact antenna test range," *Proceedings of the 27th Annual Antenna Measurement Techniques Association (AMTA) Meeting & Symposium*, Newport, RI, USA, Oct. 30 – Nov. 4, 2005, pp. 417 – 421.

[2] J. Meltaus, J. Salo, E. Noponen, M. M. Salomaa, V. Viikari, A. Lönnqvist, T. Koskinen, J. Säily, J. Häkli, J. Ala-Laurinaho, J. Mallat, and A. V. Räisänen, "Millimeter-wave beam shaping using holograms," *IEEE Transactions on Microwave Theory and Techniques*, vol. 51, no. 4, pp. 1274-1280, Apr. 2003.

[3] E. Noponen, J. Häkli, T. Koskinen, A. Lönnqvist, V. Viikari, J. Ala-Laurinaho, J. Mallat, and A. V. Räisänen, "Synthesis of reflection-type phase hologram for compact antenna test range at 310 GHz," *Proceedings of the 4th ESA Workshop on Millimetre-Wave Technology and Applications*, Espoo, Finland, Feb. 15 – 17, 2006, pp. 391 – 396.

[4] J. Salo, J. Meltaus, E. Noponen, M. M. Salomaa, A. Lönnqvist, T. Koskinen, V. Viikari, J. Säily, J. Häkli, J. Ala-Laurinaho, J. Mallat, and A. V. Räisänen, "Holograms for shaping radio-wave fields," *Journal of Optics A: Pure and Applied Optics*, pp. S161-S167, Aug. 2002.

[5] A. Lönnqvist, T. Koskinen, J. Häkli, J. Säily, J. Ala-Laurinaho, J. Mallat, V. Viikari, J. Tuovinen, and A. V. Räisänen, "Hologram-based compact range for submillimeter wave antenna testing," *IEEE Transactions on Antennas and Propagation*, vol. 53, no. 10, pp. 3151 – 3159, Oct. 2005.

[6] J. Häkli, J. Ala-Laurinaho, T. Koskinen, J. Lemanczyk, A. Lönnqvist, J. Mallat, A. V. Räisänen, J. Säily, J. Tuovinen, and V. Viikari, *IEEE Antennas and Propagation Magazine*, vol. 47, no. 5, pp. 237 – 240, Oct. 2005.

[7] J. Mallat, J. Ala-Laurinaho, V. Viikari, and A.V. Räisänen, "Dielectric-loaded flat reflector test antenna for submillimetre wave antenna measurements," *Proceedings of URSI/IEEE XXIX Convention on Radio Science*, Espoo, Finland, Nov. 1-2, 2004, pp. 123-126.

[8] A. Lerber, V. Viikari, A. Liseno, J. Ala-Laurinaho, and A.V. Räisänen, "A feasibility study of phase retrieval algorithms at sub-millimeter wavelengths," *Proceedings of the 27th Annual Antenna Measurement Techniques Association (AMTA) Meeting & Symposium*, Newport, RI, USA, Oct. 30 – Nov. 4, 2005, pp. 79 – 84.

[9] V. Viikari, J. Mallat, J. Ala-Laurinaho, J. Häkli, and A.V. Räisänen, "Antenna pattern correction in a hologram CATR based on averaging in frequency domain," *Proceedings of the 27th Annual Antenna Measurement Techniques Association (AMTA) Meeting & Symposium*, Newport, RI, USA, Oct. 30 – Nov. 4, 2005, pp. 341 – 345.

[10] V. Viikari, J. Häkli, J. Ala-Laurinaho, J. Mallat, and A. V. Räisänen, "A feed scanning based APC-technique for improving the measurement accuracy in a sub-mm CATR," *Proceedings of the 26th Annual Antenna Measurement Techniques Association (AMTA) Meeting & Symposium*, Atlanta, USA, Oct. 17–22, 2004, pp. 227–231.

[11] V. Viikari, V.-M. Kolmonen, J. Salo, and A. V. Räisänen, "Adaptive array based antenna pattern correction technique," *Proceedings of the 28th Annual Antenna Measurement Techniques Association (AMTA) Meeting & Symposium*, Austin, TX, USA, Oct. 22 – 27, 2006, pp. 368 – 372.

[12] P. de Maagt, "Terahertz technology for space and earth applications," *Proceedings of the European Conference on Antennas and Propagation*, Nice, France, Nov. 6-10, 2006, CD-rom, ESA SP-626, paper no. 431357.

[13] http://sci.esa.int/science-e/www/object/index.cfm?fobjectid=34695, Mar. 2006.

[14] J. Tuovinen, "Methods for testing reflector antennas at THz frequencies," *IEEE Antennas and Propagation Magazine*, vol. 35, no. 6, pp. 7 – 13, Dec. 1993.

[15] *IEEE Standard Test Procedures for Antennas*, ANSI/IEEE std 149-1979, 1979.

[16] P. S. Hacker and H. E. Schrank, "Range distance requirements for measuring low and ultralow sidelobe antenna patterns," *IEEE Transactions on Antennas and Propagation*, vol. AP-30, no. 5, pp. 956 – 966, 1982.

[17] A. D. Yaghjian, "An overview of near-field antenna measurements," *IEEE Transactions on Antennas and Propagation*, vol. AP-34, no. 1, pp. 30 – 45, Jan. 1994.

[18] Y. Rahmat-Samii and M. Gatti, "Far-field patterns of spaceborne antennas from plane-polar near-field measurements," *IEEE Transactions on Antennas and Propagation*, vol. 33, no. 6, pp. 638 – 648, Jun. 1985.

[19] Y. Rahmat-Samii, R. Williams, and R. Yaccarino, "The bi-polar planar near-field measurement and diagnostic facility," *Proceedings of the 8th International Conference on Antennas and Propagation*, Dallas, TX, USA, Oct. 4 – 8, 1993, pp 392 – 395.

[20] O. M. Bucci, G. Schirinnzi, and G. Leone, "A compensation technique for positioning errors in planar near-field measurements," *IEEE Transactions on Antennas and Propagation*, vol. 36, no. 8, pp. 1167 – 1172, Aug. 1988.

[21] D. Slater, *Near-field Antenna Measurements*, Norwood, MA, Artech House, 1991, 131 p.

[22] J. Säily, P. Eskelinen, and A. V. Räisänen, "Pilot signal-based real-time measurement and correction of phase errors caused by microwave cable flexing in planar near-field tests," *IEEE Transactions on Antennas and Propagation*, vol. 51, no. 2, pp. 195 – 200, Feb. 2003.

[23] A. C. Newell, "Error analysis techniques for planar near-field measurements," *IEEE Transactions on Antennas and Propagation*, vol. 36, no. 6, pp. 754 – 768, June 1988.

[24] D. Slater, P. Stek, R. Cofield, R. Dengler, J. Hardy, R. Jarnot, and R. Swindlehurst, "A large aperture 650 GHz near-field measurement system for the earth observing system microwave limb sounder," *Proceedings of the 23rd Annual Meeting & Symposium of the Antenna Measurement Techniques Association (AMTA)*, Denver, CO., USA, Oct. 21-26, 2001, pp. 468 – 473.

[25] N. Erickson and V. Tolls, "Near-field measurements of the submillimeter wave astronomy satellite antenna," *Proceedings of the 20th ESTEC Antenna Workshop on Millimetre Wave Antenna Technology and Antenna Measurements*, WPP-128, Noordwijk, The Netherlands, June 18 – 20, 1997, pp. 313 – 319.

[26] J.-C. Bolomey, B. J. Cown, G. Fine, L. Jofre, M. Mostafavi, D. Picard, J. P. Estrada, P. G. Friederich, and F. L. Cain, "Rapid near-field antenna testing via arrays of modulated scattering probes," *IEEE Transactions on Antennas and Propagation*, vol. 36, no. 6, pp. 804 – 814, June 1988.

[27] G. Junkin, T. Huang, and J. C. Bennet, "Holographic testing of terahertz antennas," *IEEE Transactions on Antennas and Propagation*, vol. 48, no. 3, pp. 409 – 417, Mar. 2000.

[28] R. G. Yaccarino and Y. Rahmat-Samii, "Phaseless bi-polar planar near-field measurements and diagnostics of array antennas," *IEEE Transactions on Antennas and Propagation*, vol. 47, no. 3, pp. 574 – 583, Mar. 1999.

[29] T. Isernia, G. Leone, and R. Pierri, "Radiation pattern evaluation from near-field intensities on planes," *IEEE Transactions on Antennas and Propagation*, vol. 44, no. 5, pp. 701 – 710, May 1996.

[30] R. Pierri, G. D'Elia, and F. Soldovieri, "A two probes scanning phaseless near-field far-field transformation technique," *IEEE Transactions on Antennas and Propagation*, vol. 47, no. 5, pp. 792 – 802, May 1999.

[31] J. E. McCormack, G. Junkin, and A. P. Anderson, "Microwave metrology of reflector antennas from a single amplitude," *Proceedings of the Institution of Electrical Engineers on Microwaves, Antennas and Propagation*, vol. 137, no. 6, pp. 276 – 284, Oct. 1990.

[32] M. D. Migliore, F. Soldovieri, and R. Pierri, "Far-field antenna pattern estimation from near-field data using a low-cost amplitude-only measurement setup," *IEEE Transactions on Instrumentation and Measurement*, vol. 49, no. 1, pp. 71 – 76, Feb. 2000.

[33] F. Las-Heras and T. K. Sarkar, "A direct optimization approach for source reconstruction and NF-FF transformation using amplitude-only data," *IEEE Transactions on Antennas and Propagation*, vol. 50, no. 4, pp. 500 – 510, Apr. 2002.

[34] R. C. Johnson, H. A. Ecker, and J. S. Hollis, "Determination of far-field antenna patterns from near-field measurements," *Proceedings of the IEEE*, vol. 61, no. 12, pp. 1668 – 1694, Dec. 1973.

[35] P. R. Foster, D. Martin, C. Parini, A. V. Räisänen, J. Ala-Laurinaho, T. Hirvonen, A. Lehto, T. Sehm, J. Tuovinen, F. Jensen, and K. Pontoppidan, "*Mmwave antenna testing techniques – Phase 2*," MAAS Report 304, Issue no. 2, ESTEC Contract no. 11641/95/NL/PB(SC), Dec. 1996, 224 p.

[36] http://www.leica-geosystems.com/corporate/en/products/laser_tracker/lgs_36108.htm, Feb 2006.

[37] P. H. Nielsen, “Grating lobes from measured Planck telescope mirrors,” *Proceeding of the 28th ESA Antenna Workshop on Space Antenna Systems and Technologies*, ESTEC, Noordwijk, The Netherlands, May 31 – June 3, 2005, pp. 627 – 631.

[38] J. Hartmann, J. Habersack, H.-J. Steiner, and J. Lemanczyk, “Comparative analysis and measurement of mm-wave applications,” *Proceedings of the 4th ESA Workshop on Millimetre-Wave Technology and Applications*, Espoo, Finland, Feb. 15 – 17, 2006, pp. 429 – 435.

[39] R. C. Johnson, H. A. Ecker, and R. A. Moore, “Compact range techniques and measurements,” *IEEE Transactions on Antennas and Propagation*, vol. AP-17, no. 5, pp. 568 – 576, Sept. 1969.

[40] A. D. Olver, “Compact antenna test ranges,” *Proceedings of the Seventh International Conference on Antennas and Propagation (ICAP)*, York, UK, 1991, pp. 99 – 108.

[41] W. D. Burnside, M. C. Gilreath, B. M. Kent, and G. L. Clerici, “Curved edge modification of compact range reflector,” *IEEE Transactions on Antennas and Propagation*, vol. 35, no. 2, pp. 176 – 182, Feb. 1987.

[42] C. W. Pistorius and W. D. Burnside, “An improved main reflector design for compact range applications,” *IEEE Transactions on Antennas and Propagation*, vol. 35, no. 3, pp. 342 – 347, Mar. 1987.

[43] G. E. Evans, *Antenna Measurement Techniques*, Artech House, Boston, 1990, 229 p.

[44] J. Häkli, J. Ala-Laurinaho, and A. V. Räisänen, “Numerical synthesis method for designing a shaped dual reflector feed system,” *Proceedings of the Institution of Electrical Engineers on Microwaves, Antennas and Propagation*, vol. 152, no. 5, pp. 311 – 318, Oct. 2005.

[45] J. Häkli, T. Koskinen, J. Ala-Laurinaho, and A. V. Räisänen, “Dual reflector feed system for hologram-based compact antenna test range,” *IEEE Transactions on Antennas and Propagation*, vol. 53, no. 12, pp. 3940 – 3948, Dec. 2005.

[46] J. R. Descardeci and C. G. Parini, “Trireflector compact antenna test range,” *Proceedings of the Institution of Electrical Engineers on Microwaves, Antennas and Propagation*, vol. 144, no. 5, pp. 305 – 310, Oct. 1997.

[47] C. R. Birtcher, C. A. Balanis, and V. J. Vokurka, “RCS measurements, transformations, and comparisons under cylindrical and plane wave illumination,” *IEEE Transactions on Antennas and Propagation*, vol. 42, no. 3, pp. 329 – 334, Mar. 1994.

[48] G. Evans, “Far field correction for short antenna ranges,” *Proceedings of the 7th Annual Antenna Measurement Techniques Association (AMTA) Meeting & Symposium*, USA, 1985, pp. 34-1 – 34-9.

[49] W. Menzel and B. Huder, “Compact range for millimeter-wave frequencies using a dielectric lens,” *Electronics Letters*, vol. 20, no. 19, pp. 768 – 769, 1984.

[50] A. D. Olver and A. A. Saleeb, “Lens-type compact antenna range,” *Electronics Letters*, vol. 15, no. 14, pp. 409 – 410, 1979.

[51] T. Hirvonen, J. Tuovinen, and A. Räisänen, "Lens-type compact antenna test range at mm-waves," *Proceedings of the 21st European Microwave Conference*, Stuttgart, Germany, vol. 2, 1991, pp. 1079 – 1083.

[52] T. Hirvonen, J. P. S. Ala-Laurinaho, J. Tuovinen, and A. V. Räisänen, "A compact antenna test range based on a hologram," *IEEE Transactions on Antennas and Propagation*, vol. 45, no. 8, pp. 1270 – 1276, Aug. 1997.

[53] J. Ala-Laurinaho, *Numerical studies on a radio frequency hologram and its use in antenna measurements*, D.Sc. dissertation, Dept. of Electrical and Communications Engineering, Helsinki University of Technology, Espoo, Finland, 2001.

[54] T. Koskinen, J. Ala-Laurinaho, J. Häkli, and A. V. Räisänen, "Studies on amplitude hologram as a submillimeter-wave collimator at circular polarisation," *Proceedings of the European Conference on Antennas and Propagation*, Nice, France, Nov. 6 – 10, 2006, CD-rom, ESA SP-626, paper no. 363576.

[55] J. Ala-Laurinaho, T. Hirvonen, P. Piironen, A. Lehto, J. Tuovinen, A.V. Räisänen, and U. Frisk, "Measurement of the Odin telescope at 119 GHz with a hologram type CATR," *IEEE Transactions on Antennas and Propagation*, vol. 49, no. 9, pp. 1264 – 1270, 2001.

[56] T. Koskinen, J. Ala-Laurinaho, J. Säily, A. Lönnqvist, J. Häkli, J. Mallat, J. Tuovinen, and A.V. Räisänen, "Experimental study on a hologram-based compact antenna test range at 650 GHz," *IEEE Transactions on Microwave Theory and Techniques*, vol. 53, no. 9, pp. 2999 – 3006, Sept. 2005.

[57] M. Paquay and J. Marti-Canales, "Pattern measurement demonstration of an untouchable antenna," *Proceedings of the 27th Annual Antenna Measurement Techniques Association (AMTA) Meeting & Symposium*, Newport, RI, USA, Oct. 30 – Nov. 4, 2005, pp. 21 – 26.

[58] J. Appel-Hansen, "Accurate determination of gain and radiation patterns by radar cross-section measurements," *IEEE Transactions on Antennas and Propagation*, vol. AP-27, no. 5, pp. 640 – 646, Sept. 1979.

[59] J. D. Kraus, "Holographic measurements," in *Radio Astronomy*, 2nd ed. Ohio/USA, Cygnus-Quasar Books, 1986, Chapter 6-22, pp. 6-63 – 6-67.

[60] O. M. Bucci, G. D'Elia, and G. Romito, "Reflector distortions diagnosis from far-field amplitude pattern," *IEEE Transactions on Antennas and Propagation*, vol. 43, no. 11, pp. 1217 – 1225, Nov. 1995.

[61] J. W. M. Baars, J. Magnum, and R. Lucas, "Near-field radio-holography of the ALMA prototype antennas at 3 mm wavelength," *Proceeding of the 28th ESA Antenna Workshop on Space Antenna Systems and Technologies*, ESTEC, Noordwijk, The Netherlands, May 31 – June 3, 2005, pp. 861 – 864.

[62] J. C. Bennet and A. Griziotis, "Removal of environmental effects from antenna radiation patterns by deconvolution processing," *Proceedings of the IEE Conference,* Pub. 219, Pt. 1, 1983, pp. 224 – 228.

[63] A. A. Saleeb, A. D. Olver, and M. G. T. El-Kholy, "Extraction of the true radiation pattern of a microwave antenna from measurements in a noisy environment," *Digest of Antennas and Propagation Society International Symposium*, Chicago, IL, USA, July 18 – 25, 1992, pp. 2052 – 2055.

[64] P. L. Garcia Muller, J. L. Cano, and R. Torres, "A deconvolution method for correcting antenna measurement errors in compact antenna test ranges," *Proceedings of the 17th Annual Antenna Measurement Techniques Association (AMTA) Meeting & Symposium*, Williamsburg, VA, USA, Nov. 13 – 17, 1995, pp. 509 – 514.

[65] D. N. Black and E. B. Joy, "Test zone field compensation," *IEEE Transactions on Antennas and Propagation*, vol. 43, no. 4, pp. 362 – 368, Apr. 1995.

[66] D. A. Leatherwood and E. B. Joy, "Plane wave, pattern subtraction, range compensation," *IEEE Transactions on Antennas and Propagation*, vol. 49, no. 12, pp. 1843 – 1851, Dec. 2001.

[67] R. E. Hiatt, E. F. Knott, and T. B. A. Senior, "A study of VHF absorbers and anechoic rooms," Radiation Laboratory, University of Michigan, Technical Report 5391-1-F, 1963.

[68] A. M. Predoehl and W. L. Stutzman, "Implementation and results of a time-domain gating system for a far-field range", *Proceedings of the 19th Annual Meeting & Symposium of the Antenna Measurement Techniques Association (AMTA)*, Boston, MA, USA, Nov. 17 – 21, 1997, pp. 8–12.

[69] B. Fourestie, Z. Altman, and M. Kanda, "Anechoic chamber evaluation using the matrix pencil method," *IEEE Transactions on Electromagnetic Compatibility*, vol. 41, no. 3, pp.169 – 174, Aug. 1999.

[70] B. Fourestie, Z. Altman, J. Wiart, and A. Azoulay, "On the use of the matrix-pencil method to correlate measurements at different test sites," *IEEE Transactions on Antennas and Propagation*, vol. 47, no. 10, pp. 1569 – 1573, Oct. 1999.

[71] T. Sarkar and O. Pereira, "Using the matrix pencil method to estimate the parameters of a sum of complex exponentials," *IEEE Antennas and Propagation Magazine*, vol. 37, no. 1, pp. 48 – 55, Feb. 1995.

[72] B. Fourestie and Z. Altman, "Gabor schemes for analyzing antenna measurements," *IEEE Transactions on Antennas and Propagation*, vol. 49, no. 9, pp. 1245 – 1253, Sept. 2001.

[73] P. S. H. Leather and D. Parsons, "Equalization for antenna-pattern measurements: established technique – new application," *IEEE Antennas and Propagation Magazine*, vol. 45, no. 2, pp. 154 – 161, Apr. 2003.

[74] J. Appel-Hansen, "Reflectivity level of radio anechoic chambers," *IEEE Transactions on Antennas and Propagation*, vol. AP-21, no. 4, pp. 490 – 498, July 1973.

[75] W. D Burnside and I. J. Gupta, "A method to reduce signal errors in antenna pattern measurements," *IEEE Transactions on Antennas and Propagation*, vol. 42, no. 3, pp. 399 – 405, Mar. 1994.

[76] R. L. Mitchell, "On the reduction of stray signal errors in antenna pattern measurements," *IEEE Transactions on Antennas and Propagation*, vol. 43, no. 6, pp. 629 – 630, June 1995.

[77] J. van Norel and V. J. Vokurka, "Novel APC-methods for accurate pattern determination," *Proceedings of the 15th Annual Antenna Measurement Techniques Association (AMTA) Meeting & Symposium*, USA, 1993, pp. 385 – 389.

[78] I. Kåsa, "A circle fitting procedure and its error analysis," *IEEE Transactions on Instrumentation and Measurement*, vol. 25, pp. 8 – 14, Mar. 1976.

[79] C. A. Corral and C. S. Lindquist, "On implementing Kåsa's circle fit procedure," *IEEE Transactions on Instrumentation and Measurement*, vol. 47, no. 3, pp. 789 – 795, June 1998.

[80] J. van Norel, A. H. van Gastel, V. J. Vokurka, J. Neve, and J. F. Coroller, "Application of flexible scanning in advanced APC-techniques," *Proceedings of the 16th Annual Antenna Measurement Techniques Association (AMTA) Meeting & Symposium*, USA, 1994, pp. 411 – 415.

[81] M. D. Migliore, "Filtering environmental reflections in far-field antenna measurement in semi-anechoic chambers by an adaptive pattern strategy," *IEEE Transactions on Antennas and Propagation*, vol. 52, no. 4, pp. 1112 – 1115, Apr. 2004.

[82] T. J. Shan, M. Wax, and T. Kailath, "On spatial smoothing for estimation of coherent signals," *IEEE Transaction on Acoust., Speech, Signal Prcessing*, vol. ASSP-33, pp. 806 – 811, Aug. 1985.

[83] I. J. Gupta, "Stray signal source location in far-field antenna/RCS ranges," *IEEE Antennas and Propagation Magazine*, vol. 46, no. 3, pp. 20 – 29, June 2004.

[84] T. P. Delfeld and F. C. Delfeld, "Use of the MUSIC algorithm in the analysis of compact range field probe data," *Proceedings of the 11th Annual Antenna Measurement Techniques Association (AMTA) Meeting & Symposium*, Monterey, CA, USA, Oct. 9 – 13, 1989, pp. 6-3 – 6-9.

[85] I. J. Gupta and W. D. Burnside, "Imaging the compact range probe data," *Proceedings of the 12th Annual Antenna Measurement Techniques Association (AMTA) Meeting & Symposium*, Philadelphia, PA, USA, 1990, pp. 14-13 – 14-17.

[86] R. O. Scmidt, "Multiple emitter location and signal parameter estimation," *IEEE Transactions on Antennas and Propagation*, vol. 34, no. 3, pp. 276 – 280, Mar. 1986.

[87] A. Moghaddar and E. K. Walton, "Imaging of low level signals in a compact range," *Proceedings of the 12th Annual Antenna Measurement Techniques Association (AMTA) Meeting & Symposium*, Philadelphia, PA, USA, 1990, pp. 14-3 – 14-8.

[88] A. van der Merwe and D. J. Janse van Rensburg, "Main-beam reduction for compact range imaging," *Proceedings of the Institution of Electrical Engineers on Microwaves, Antennas and Propagation*, vol. 141, no. 6, pp. 461 – 463, Dec. 1990.

[89] T. D. Moore and I. J. Gupta, "Calibration of range probe data for stray signal analysis," *Proceedings of the 22nd Annual Antenna Measurement Techniques Association (AMTA) Meeting & Symposium*, Philadelphia, PA, USA, Oct. 16 – 20, 2000, pp. 228 – 233.

[90] M. Boumans and H. Eriksson, "Sidelobe accuracy improvement in a compact range using multiple feed locations," *Proceedings of the 27th Annual Antenna Measurement Techniques Association (AMTA) Meeting & Symposium*, Newport, RI, USA, Oct. 30 – Nov. 4, 2005, pp. 408 – 412.

[91] O. M. Bucci, G. Franceschetti, G. Mazzarella, and G. Panariello, "Intersection approach to array pattern synthesis," *Proceedings of the Institution of Electrical Engineers on Microwaves, Antennas and Propagation*, vol. 137, no. 6, pp. 349 – 357, Dec. 1990.

[92] E. Botha and D. A. McNamara, "Conformal array synthesis using alternating projections, with maximal likelihood estimation used in one of the projection operators," *IEE Electronics Letters*, vol. 29, no. 20, pp. 1733 – 1734, Sep. 1993.

[93] E. D. Dufort, "Pattern synthesis based on adaptive array theory," *IEEE Transactions on Antennas and Propagation*, vol. 37, no. 8, pp. 1011 – 1018, Aug. 1989.